# Antarctic atmospheric Richardson number from radiosoundings measurements and AMPS

Qike Yang[1,2,3], Xiaoqing Wu[1,2,3], Xiaodan Hu[1,2,3], Zhiyuan Wang[1,3], Chun Qing[1,2,3], Tao Luo[1,2,3], Pengfei Wu[1,2,3], Xianmei Qian[1,2,3], Yiming Guo[1,2,3]

[1]Key Laboratory of Atmospheric Optics, Anhui Institute of Optics and Fine Mechanics, HFIPS, Chinese Academy of Sciences, Hefei 230031, China
[2]Science Island Branch of Graduate School, University of Science and Technology of China, Hefei 230026, China
[3]Advanced Laser Technology Laboratory of Anhui Province, Hefei 230037, China

*Correspondence to*: Xiaoqing Wu (xqwu@aiofm.ac.cn)

**Abstract.** Monitoring a wide range of atmospheric turbulence over the Antarctic continent is still tricky, while the atmospheric Richardson number ($Ri$; a ~~critical~~valuable parameter ~~determining~~which determines the possibility ~~of~~that turbulence could be triggered) is easier to obtain. The Antarctic atmospheric $Ri$, calculated ~~using~~from the potential temperature and wind speed, was investigated using the daily results from the radiosoundings and forecasts of the Antarctic Mesoscale Prediction System (AMPS). Radiosoundings for a year at three sites (McMurdo, South Pole, and Dome C) were used to quantify the reliability of the AMPS forecasts. The AMPS-forecasted $Ri$ ~~(inverse of the Richardson number)~~ can identify the main spatiotemporal characteristics of atmospheric turbulence over the Antarctic ~~continent in terms of space and time.~~region. The correlation coefficients ($R_{xy}$) of $\log_{10}(Ri)$ at McMurdo, the South Pole, and Dome C are 0.71, 0.~~66~~59, and 0.~~68~~53, respectively. The $Ri$ ~~, where~~ was generally underestimated by the ~~performance gains during the warm seasons. In addition, a model to improve~~ AMPS~~-forecasted has been presented. The monthly median at~~ and the AMPS could better capture the trend of $\log_{10}(Ri)$ ~~three sites and the~~ under relatively unstable atmospheric conditions. The seasonal median of $\log_{10}(Ri)$ ~~throughout the~~ along two vertical cross-sections ~~for~~of the AMPS forecasts are presented~~. One can observe that the probability of triggering~~, and it shows some zones where atmospheric turbulence can be highly triggered in Antarctica. The $\log_{10}(Ri)$ ~~is primarily concentrated near the ground. In addition, strong wind shears near escarpment regions have been found in the range of 0-5 km above the ground, thus causing atmospheric instability (or a thick boundary layer). In addition, turbulent atmospheres are likely~~ distributions appear to be reasonably correlated to ~~be triggered~~ some large-scale phenomena or local-scale dynamics (katabatic winds, polar vortices, convection, gravity wave, etc) over the ~~ocean, moving toward the~~ Antarctic ~~Plateau~~plateau and ~~becoming stable.~~surrounding ocean. Finally, the $\log_{10}(Ri)$ at the planetary boundary layer height ($PBLH$ ~~), , has been provided as a reference standard for judging atmospheric stability. The~~) were calculated and their median value ~~of from the combined data of two vertical cross-sections was 0.55, which~~is 0.316, this median value, in turn, was used to ~~calculate~~estimate $PBLH$ and agree well with the AMPS-forecasted $PBLH$ ($R_{xy} \geq 0.69$). Overall, our results suggest that the estimated $\log_{10}(Ri)$ ~~forecasts (>0.72).~~ by AMPS are reasonable and the turbulence conditions in Antarctica are well revealed.

## 1 Introduction

The Richardson number ($Ri$) is a valuable parameter for giving insight into atmospheric stability ~~monitoring~~; it combines both thermodynamic and dynamic profiles~~—~~, which provides us with valuable insights into turbulent heat fluxes (Town and Walden,

2009) and the probability that optical turbulence (Yang et al., 2021; Yang et al., 2022) can be triggered in Antarctica. However, the measurements of atmospheric properties in Antarctica are sparse compared to those in the mid-latitudes and tropics. Atmospheric models have been developed to overcome this limitation (Meso-NH by Lascaux et al., 2009; Polar WRF by Bromwich et al., 2013; MAR by Gallée et al., 2015), allowing researchers to investigate atmospheric variability beyond observational coverage, even for forecasting atmospheric propertiesparameters in the future.

The Antarctic Mesoscale Prediction System (AMPS; https://www2.mmm.ucar.edu/rt/amps/) runs a real-time atmospheric model and provides numerical forecasts for Antarctica. The performances of AMPS in forecasting temperature, wind, precipitable water vapor, cloud, radiation, and heat flux have been examined in previous studies (Monaghan et al., 2005; Seefeldt et al., 2011; Vázquez B and Grejner-Brzezinska, 2012; Wille et al., 2016; Listowski and Lachlan-Cope, 2017; Hines et al., 2019). To our knowledge, using the AMPS to forecast $Ri$ has not been formally validated. Thus, this study will investigate the reliability of the estimated $Ri$ of Antarctica. The atmospheric model employed for AMPS is a using AMPS forecasts. The atmospheric model employed for AMPS is the Polar version of the Weather Research and Forecasting (Polar WRF) model (Powers et al., 2012). Polar WRF (http://polarmet.osu.edu/PWRF/) has been modified for use in polar regions, for example, improving the representation of heat transfer through snow and ice (Hines and Bromwich, 2008; Hines et al., 2015). The Polar WRF has been used to simulate the $Ri$ at Dome A in Antarctica, and the simulated $Ri$ basically behaved as expected as the $Ri$ is generally large when the atmosphere is less turbulent (corresponding to the measured astronomical seeing is small; Yang et al., 2021) and performed well in estimating boundary layer height when compared with other methods (Yang et al., 2022). The Polar WRF model was developed and maintained by the Polar Meteorology Group of the Byrd Polar and Climate Research Center (). The simulated by Polar WRF seems to be reasonable in Antarctica when compared to an atmosphere turbulence parameter . In addition, various verification studies of the AMPS have been conducted . However, previous verification studies have concentrated on and around the Ross Ice Shelf (or just a part of Antarctica), which needs to be extended..

And so farPresently, monitoring a wide range of atmospheric turbulence over the Antarctic continent is still tremendoustremendously difficult at present, while the, but atmospheric $Ri$ Richardson number (; a critical parameter judging the possibility of the turbulence could be triggered) is easier to obtain, as it can be calculated byfrom the routine meteorological parameters (potential temperature and wind speed). However, a precise evaluation offew studies have evaluated atmospheric models to forecast $Ri$ atmospheric in Antarctica is sketchy., because of limited meteorological experiments here. Nevertheless, Geissler and Masciadri (2006) and Hagelin et al. (2008)the analyses from used the European Centre for Medium-Range Weather Forecasts (ECMWF) have been used analyses to calculate atmospheric $Ri$ in Antarctica. The ECMWF analyses were generated from the data assimilation using observations (P. Lönnberg, 1992) (the inverse of the Richardson number) by and ., and can provide initial states for numerical models (such as Polar WRF). However, their researches have research has some specific shortagesshortcomings (or problems that need further study): (1) They did not compare $Ri$ A direct comparison of between the model estimations andfrom measurements has not been conducted. (2) Evaluations of forecast ability have not been done yetand forecasts, while the forecast function is of great significance for practical application. (3) Variability (e.g., astronomical observations, aviation safety, optical communication, etc). (2) How model error of $Ri$ at high horizontal spatial resolution has not been given, as previous studies focus depends on atmospheric conditions has not been analyzed. (3) The correlations between turbulence conditions (indicated by $Ri$ profiles at separate sites.) and some large-scale phenomena or local-scale dynamics in Antarctica were not fully investigated. (4) A reasonable reference standard for judging the atmospheric stability byprobability of triggering turbulence using the model estimations estimated $Ri$ was not given. To fill these gaps, the scientific goals of this paper are thus as follows.:

1. To carry out a detailed comparison of ~~the~~potential temperature and wind speed (on which $Ri$ depends) in the atmospheric column, this study extends the model evaluations ~~performed by~~above two sites (Hagelin et al., 2008)~~ above two sites~~ to three sites (McMurdo, South Pole, and Dome C) over the Antarctic continent for ~~a~~an entire year. The three sites are considered representative, as the coast (McMurdo), flank (South Pole), and summit (Dome C) of the Antarctic continent will be compared using radiosoundings and AMPS forecasts.

2. The radiosonde can measure meteorological parameters, which can estimate $Ri$ . Using the AMPS-forecasted meteorological parameters, ~~we~~one also can obtain the $Ri$ ~~AMPS-forecasted . The measured will also be calculated using the radiosounding-measured meteorological parameters.~~. Then, a ~~direct~~ comparison of $Ri$ ~~between~~ estimated from measurements and forecasts can be achieved, allowing us to evaluate the reliability of AMPS-forecasted $Ri$ ~~ability of the AMPS to forecast~~ in giving insight into the atmospheric ~~stability or instability.~~turbulence in Antarctica. In addition, we ~~investigate~~investigated how ~~to correct~~ the discrepancies between the ~~AMPS-forecasted~~ models and ~~obtain a result closer to the~~ measurements depend on the atmospheric conditions.

~~-~~3. ~~We also extended the analysis of done by for three sites to two~~Two vertical cross-sections for $Ri$ ~~at a high horizontal resolution. Finally,~~ will be given, which may provide a better perspective on the turbulence conditions in both vertical and horizontal dimensions, instead of only focusing on the vertical dimension (or atmospheric column; e.g., Hagelin et al. 2008 and Geissler and Masciadri 2006). This will help to identify regions and periods that are ~~favourable~~favorable for triggering atmospheric turbulence ~~(or instability) can be identified. Thus, this study provides a better perspective on atmospheric dynamics~~ in Antarctica.

~~4. To demonstrate the practicality of the AMPS-forecasted and provide more information about the atmospheric properties over the Antarctic continent, the planetary boundary layer (PBL) height, , forecasted by the AMPS, is used~~ Moreover, this will enable us to correlate the $Ri$ ~~compare~~ distribution with ~~the AMPS-forecasted . can~~some large-scale phenomena or local-scale dynamics (katabatic winds, polar vortices, convection, gravity wave, etc.) in Antarctica, and the underlying physical processes of Antarctic atmospheric turbulence will be investigated.

4. The Planetary Boundary Layer Height ( $PBLH$ , within which the atmosphere is generally turbulent) can be estimated ~~where decreases to~~ using a critical value of $Ri$ , typically 0.25 (Holtslag et al., 1990; Pietroni et al., 2012; Petenko et al., 2019). However, this critical value depends on the vertical resolution of data (Troen and Mahrt, 1986; Holtslag et al., 1990)~~, denoted by .~~, and may be different for the AMPS grid resolution. Then~~,~~ the $Ri$ ~~(i.e.~~ at the AMPS-forecasted $PBLH$ ( $Ri_{PBLH}$ ~~PBL height)~~) was obtained as a reference standard for judging whether the atmosphere is likely to be laminar flow ( $Ri \geq Ri_{PBLH}$ ~~was stable~~) or turbulent flow ( $Ri < Ri_{PBLH}$ ~~) or unstable (>~~) when using the AMPS-forecasted $Ri$ .

In Sect. 2, we present the experimental data and atmospheric model used in this study, with an explanation of their main characteristics. In Sect. 3, the Richardson number is introduced. In Sect. 4, we compare AMPS forecasts to radiosoundings and ~~analyse~~analyze the atmospheric ~~properties~~turbulence conditions in Antarctica. Sect. 5 ~~discusses the relationship between the distribution and typical atmospheric features in Antarctica. Sect. 6 summarises~~summarizes the main ~~aspects~~findings and primary takeaways of this study.

## 2 Data and model

### 2.1 Radiosoundings

Daily radiosounding measurements at McMurdo (MM) and South Pole (SP) are available at the Antarctic Meteorological Research Center (AMRC; ftp://amrc.ssec.wisc.edu/pub). For Dome C (DC), one can ~~access~~obtain the measurements at the Antarctic Meteo-Climatological Observatory (http://www.climantartide.it). The altitudes of the three sites are 9 m (MM), 2839 m (SP), and 3239 m (DC), where the altitudes correspond to the ~~height~~heights of the ~~radiosoundings~~radiosondes at the time of launch. Their locations are shown in Fig. 1. Dome A (DA) is also marked in Fig. 1, which is the highest location (4083 m) on the Antarctic plateau, and the atmospheric conditions above it will also be analyzed in this study (Sect. 4.2.3). The ~~radiosounding~~radiosonde-measured meteorological parameters include pressure, temperature, wind speed, and wind direction~~.~~ ~~This study used~~ ; one year ~~of data~~ (from 2021 March ~~2021~~ to 2022 February) of these meteorological parameters was used in this study. Generally, the radiosonde was launched once a day at the same hour (sometimes twice a day at MM and SP). In total, 518, 508, and 340 profiles were available at MM, SP, and DC from March 2021 to February 2022.

Table 1. Main technical specifications of the radiosonde RS41.

| Measuring element | System resolution | System uncertainty | Data resolution[a] |
|---|---|---|---|
| Temperature | 0.01 °C | 0.15 °C (> 100 hPa)<br>0.30 °C (<100 hPa) | 0.1 °C |
| Pressure | 0.01 hPa | 0.5 hPa (> 100 hPa)<br>0.3 hPa (3-100 hPa) | 0.1 hPa |
| Wind speed | 0.1 $ms^{-1}$ | 0.15 $ms^{-1}$ | 0.1 $ms^{-1}$ (McMurdo)<br>0.1 kts (South Pole)<br>0.1 $ms^{-1}$ (Dome C) |
| Wind Direction | 0.1 deg | 2 deg | 0.1 deg (McMurdo)<br>1 deg (South Pole)<br>1 deg (Dome C) |

[a] Resolution in the files that are available for download from the Web (ftp://amrc.ssec.wisc.edu/pub, http://www.climantartide.it ~~2022).~~ ).

The radiosonde instrumentation used during this measurement period was the Vaisala RS41 (Technical data: https://www.vaisala.com/en/products/weather-environmental-sensors/upper-air-radiosondes-rs41). The accuracy and uncertainty of the radiosonde measurements are listed in Table 1. Vaisala RS41 radiosondes have gradually replaced an older version (Vaisala RS92) starting in late 2013. These two radiosondes agree well with global average temperature differences <0.1-0.2 K in the lower stratosphere, but RS41 appears to be less sensitive than RS92 to changes in solar elevation angle (Sun et al., 2019). Besides, RS41 (1-1.5% dry bias) has better performance than RS92 (3-4% dry bias) relating to the infrared atmospheric sounding interferometer as a practical reference (Sun et al., 2021). Near-global radiosonde measurements have been used to calculate the Richardson number and derive the boundary layer height, which is positively correlated with the results of four reanalysis products (Guo et al., 2021)~~radiosounding measurements are listed in Table 1. The balloon scans the atmosphere between the ground and an altitude of 10–25 km (low in winter and high in summer); the vertical resolution is approximately 5 m, depending on the ascent speed.~~.

In Antarctica, the radiosondes measure the atmosphere between the ground and an altitude of 10–25 km (low in winter and high in summer) with a typical ascent rate of 5 m $s^{-1}$, and a logging frequency of 1 Hz; then the vertical resolution is approximately 5 m.

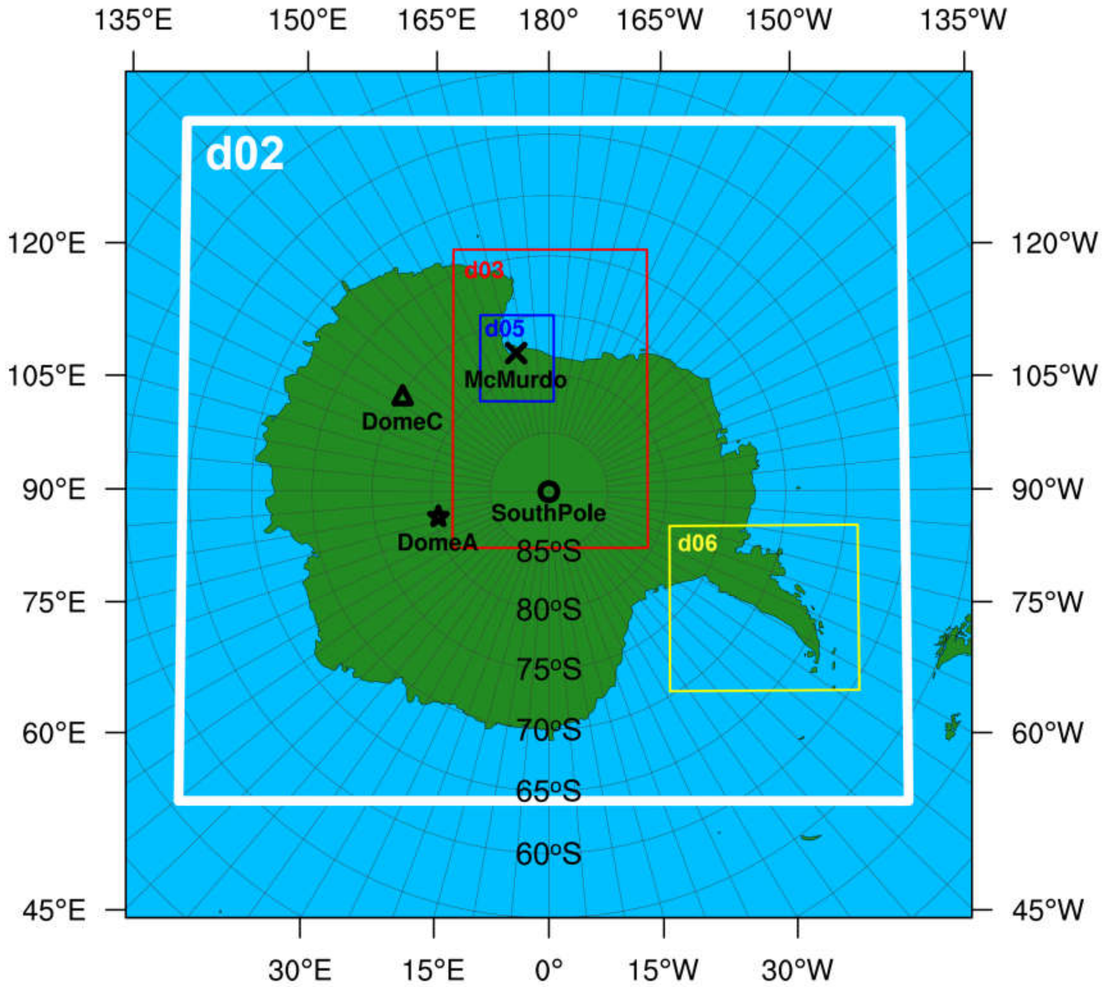


Figure 1. The five two-way interactive horizontal grids (d01, d02, d03, d05, and d06; information online at https://www2.mmm.ucar.edu/rt/amps/information/configuration/maps_2017101012/maps.html

~~Table 1. Main technical specifications of the radiosonde instrumentation.~~

~~[a] Resolution in the files that are available for download from the Web.~~

) used in the AMPS configuration. The locations of McMurdo (78°S, 167°E), South Pole (90°S, …°E), Dome C (75°S, 123°E), and Dome A (80°S, 78°E) are shown by the cross, circle, triangle, and star, respectively. This study used grid 2 fields (d02; the white rectangle) that covered the entire Antarctic continent.

## 2.2 AMPS

The AMPS can forecast meteorological parameters in four-dimensional space-time in Antarctica, which can be used for comparison with the radiosonde measurements ~~of radiosoundings~~. The AMPS grid system consisted of a series of nested domains with 60 vertical levels. This study used grid 2 fields (d02; 8 km horizontal resolution) that covered the entire Antarctic continent (similar to Hines et al., 2019), as shown by the white square in Fig. 1. However, the contributions from the nested grid with higher horizontal resolution (d03: 2.67 km; d05: 0.89 km; d06: 2.67 km) are not entirely lost, as the AMPS used a two-way nested run and the nest (e.g. d03) feeds its calculation back to the coarser domain (e.g. d02). The original WRF output files for each AMPS grid were saved in a rolling archive (one can find how to ~~access~~download the original WRF output files ~~of AMPS for each grid~~ at https://www2.mmm.ucar.edu/rt/amps/information/amps_esg_data_info.html). This study used the AMPS outputs (in original WRF format) ~~for forecast hours 12-21 at three h intervals~~ from the daily AMPS forecasts that began at 12:00 UTC. Parish and Waight (1987)~~Thus, our AMPS~~ showed large adjustments to the boundary layer fields ~~had a spin-up time of 12 h . Finally, the AMPS forecasts for~~above an ice sheet before the ~~same period (from March 2021~~numerical model began to stabilize after about 10 h. Then, some studies (Hines and Bromwich, 2008; Hines et al., 2019) have discarded the first 12 h forecasts (so-called 12 h spin-up time). Thus, in this study, only the 12-33-h forecasts from each of the AMPS simulations are combined into a year-long (2011 March to 2022 February~~ 2022), as the used radiosounding measurements, were downloaded for analysis)~~ output field at 3-h intervals.

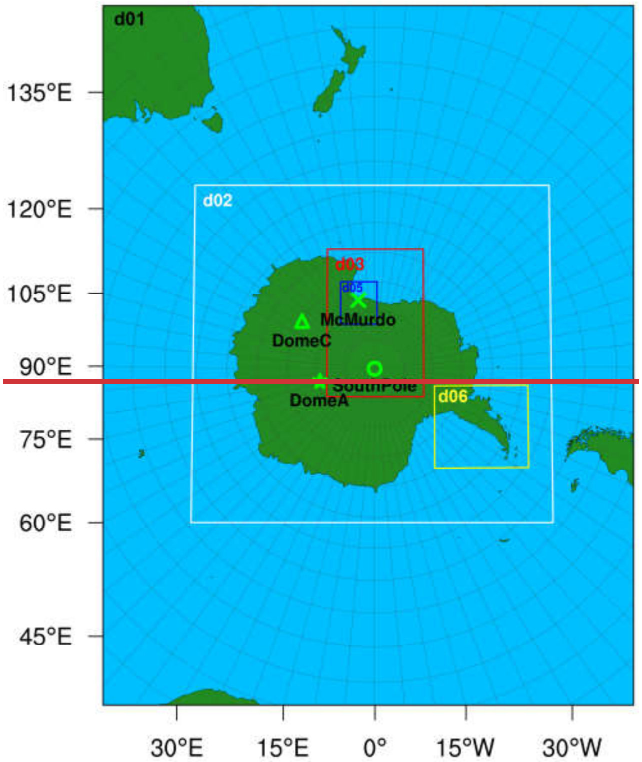


~~Figure 1. The five two-way interactive horizontal grids (d01, d02, d03, d05, and d06; information online at ) used in the AMPS configuration. The locations of McMurdo (78°S, 167°E), South Pole (90°S, …°E), Dome C (75°S, 123°E), and Dome A (80°S, 78°E) are shown by the cross, circle, triangle, and star, respectively.~~

## 3 Theory of Richardson number

The ~~stability of the atmosphere can be estimated using the~~ Richardson number ( $Ri$ ~~)~~) is generally defined as (Richardson and Shaw, 1920; Chan, 2008):

$$Ri = \frac{g}{\theta}\frac{\partial\theta/\partial z}{[\partial u/\partial z]^2 + [\partial v/\partial z]^2}, \quad (1)$$

whereWhere $g$ is the gravitational acceleration (9.8 m s$^{-2}$), $\theta = T\left[1000/P\right]^{0.286}$ is the potential temperature (K), $T$ and $P$ is are the temperature (K) and pressure (hPa) of air, respectively. As for wind shear term, $u$ and $v$ are the east-west and north-south components of the wind ( $\mathrm{m\,s^{-1}}$). $z$ is the height (m) above the ground. To calculate $Ri$ (m s-, a centered finite difference operation was used to estimate the gradient in Eq. (1).

The productiondevelopment of atmospheric turbulence (or unstable atmosphere) was shown to be tightly correlated with the $Ri$. It can, therefore, be an essential indicator of the turbulence characteristics in the atmosphere (Ma et al., 2020; Han et al., 2021; Yang et al., 2021). Atmospheric conditions are favourablefavorable for the occurrence of turbulence when $Ri$ is less than a critical value ( $Ri_c$ ; critical Richardson number).), and $Ri_c$ is typically chosen as 0.25; however. However, a larger $Ri_c$ should be used in a large-scale model (e.g., 0.5 has been employed by Troen and Mahrt, 1986).

In the results of this study, the logarithm of $Ri$, $\log_{10}\left(Ri\right)$, is presented instead of $Ri$ itself, because $Ri$ In this study, the inverse of the Richardson number () was used to provide better evidence of atmospheric stability, as in and . The larger the , the higher the probability of triggering turbulence in the atmosphere.

can vary by two or more orders of magnitude in the atmosphere.

## 4 Results and discussion

### 4.1 TemperaturePotential temperature and wind speed

The AMPS forecasts are compared to radiosoundings from MM, SP, and DC to investigate the reliability of the AMPS forecasts over the Antarctic continent. The AMPS forecasts and radiosoundings used for this comparison were obtained from March 2021 to February 2022. To offer a more convincing result, data corresponding to the altitude at which radiosoundings reached less than five times a monthseason were discarded. In addition, the extracted AMPS forecasts used for comparison were from the nearest grid to the three sites, and the time difference between radiosoundings and AMPS forecasts and radiosoundings larger than 1.5 hours was also not used for comparison. Moreover, both radiosoundings and AMPS forecasts and radiosoundings were linearly interpolated to the same height series (average annual altitude of the AMPS vertical grid, because; where the altitude of the AMPS grid may vary during the simulation as the AMPS uses the WRF hybrid vertical coordinate, information online at https://www2.mmm.ucar.edu/wrf/users/docs/user_guide_v4/WRFUsersGuide.pdf) for each site. On the other hand, it should be noted that the near-surface radiosonde measurements could be less reliable, as it was just released from the operator's hand (or some machine). Hagelin et al. (2008) conclude that the radiosoundings are ~1 K colder than the Automatic Weather Station at Dome C and ~2 K at the South Pole. In this study, the radiosonde measurements in the first ~10 m above the ground are not used. This is also because the first AMPS grid is ~10 m above the ground.

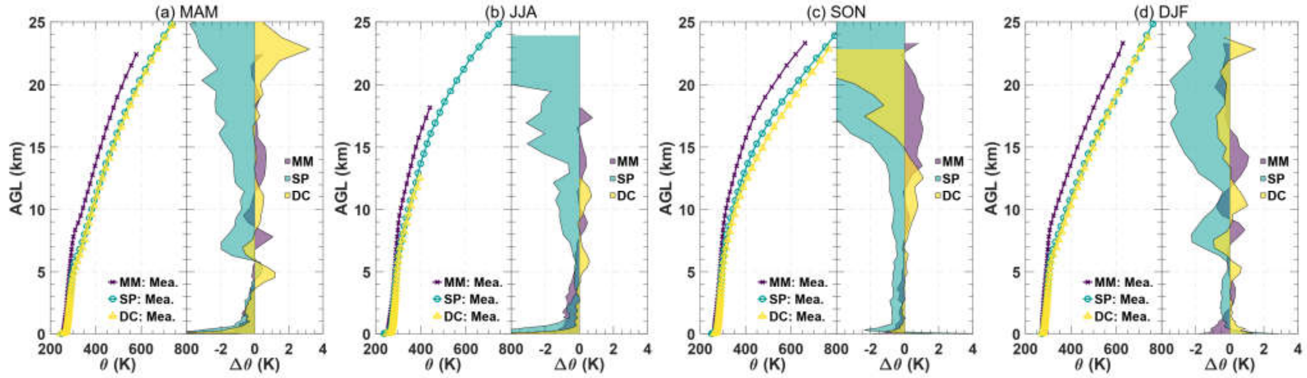


Figure 2. The ~~monthly medians~~ seasonal median of ~~the~~potential temperature ( $\theta$ ~~differences (Fig. 2)~~) estimated by the radiosonde measurements (solid lines) and potential temperature difference ( $\Delta\theta$ ~~wind speed (Fig. 3) between~~ ) calculated by the AMPS forecasts ~~and radiosoundings are presented. The panels in~~ minus the radiosonde measurements, i.e. $\Delta\theta = \theta_{AMPS} - \theta_{Mea.}$ ~~same row of Figs. 2 and 3 correspond to the same season; the first row: Aut. (Autumn~~ (filled areas). Fall: March~~, April, and~~ -May~~), second row: Win. (Winter~~ (MAM); winter: June~~, July, and~~ -August~~), third row: Spr. (Spring~~ (JJA); spring: September~~, October, and~~ -November~~), fourth row: Sum. (Summer~~ (SON); summer: December~~, January, and~~ -February (DJF).

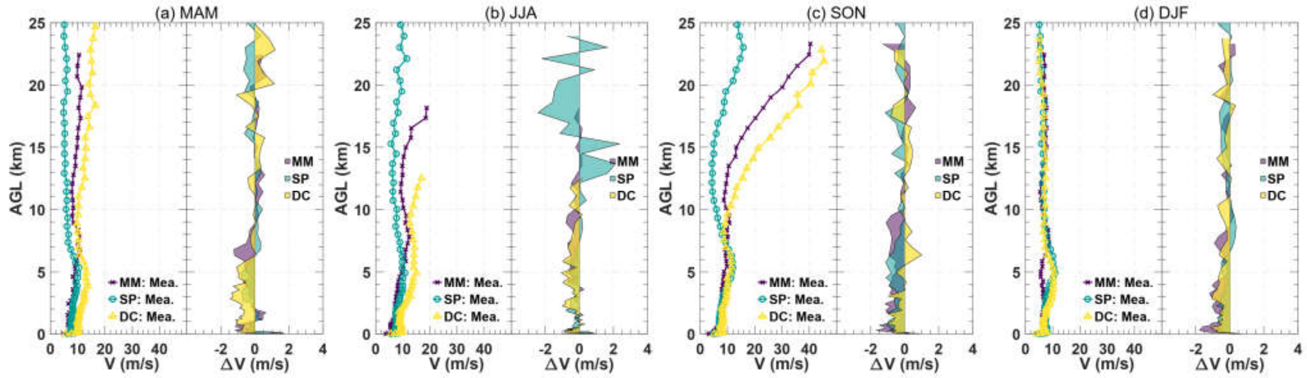


Figure 3. As in Fig 2, but for wind speed $V$ $(= \sqrt{u^2 + v^2}$ ), and $\Delta V = V_{AMPS} - V_{Mea.}$ ~~).~~ .

The seasonal median difference of potential temperature (see the filled areas in Fig. 2) and wind speed (see the filled areas in Fig. 3) between radiosoundings and the AMPS forecasts are presented. The missing value of ~~the~~ median difference in the upper part of the atmosphere during JJA indicates that the ~~radiosoundings do~~radiosonde balloon does not reach as high an AGL (Above Ground Level) in winter as they do in summer, probably because the elastic material of the balloons is more fragile in cold seasons and easier to explode (Hagelin et al., 2008). The lack of measurements may also be attributable to some large values of the median difference in the top layer of the profile shown in Figs. ~~2 and 3.~~2 and 3, as the AMPS requires the assimilation data from measurements to initialize its numerical model, and the lack of measurements makes it more difficult for AMPS to simulate atmospheric changes that are close to reality.

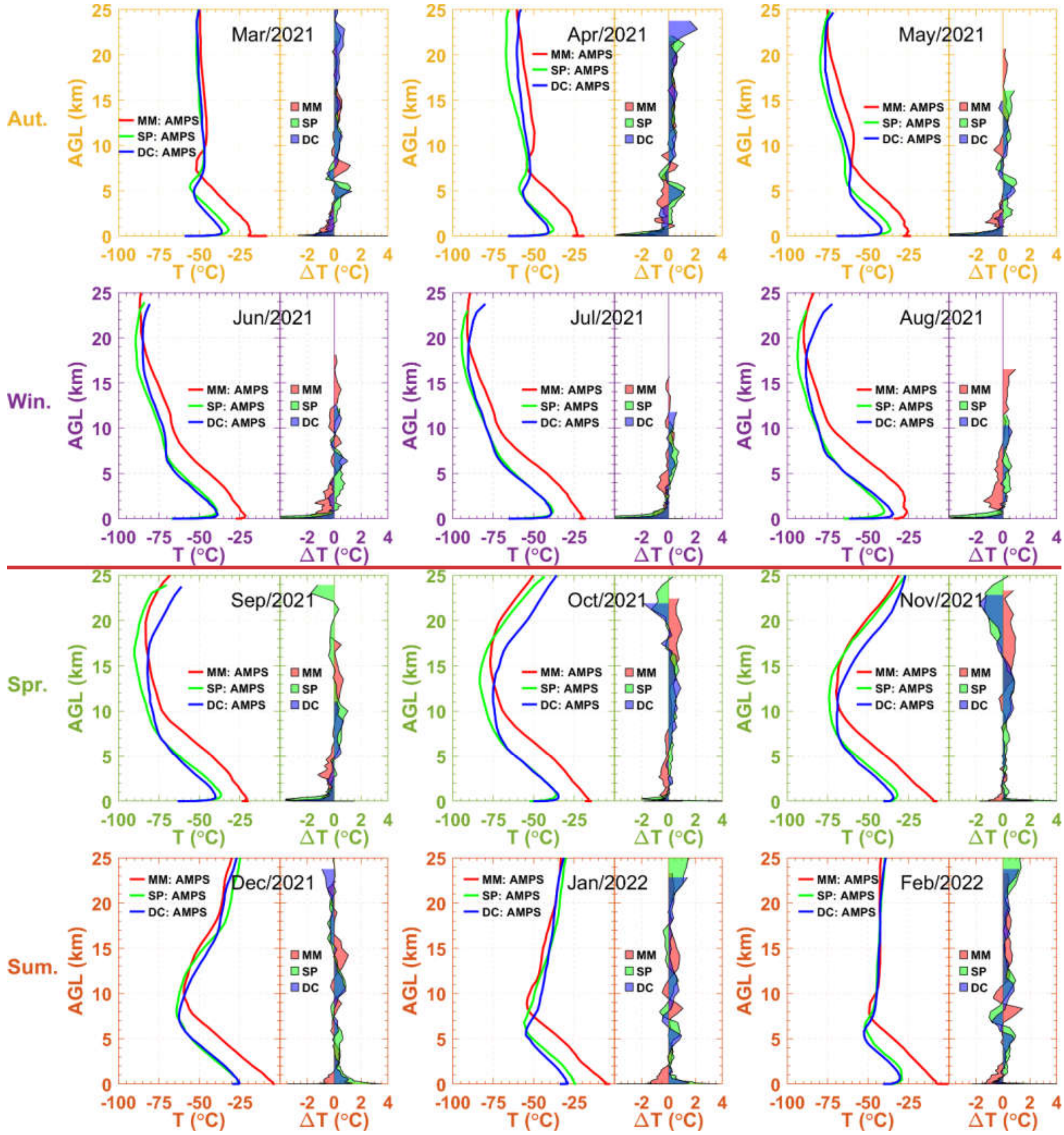


Figure 2. The monthly median for temperature forecasted by the AMPS (solid lines) and temperature difference calculated by the AMPS forecasts minus the radiosoundings measurements, i.e.  (filled areas).

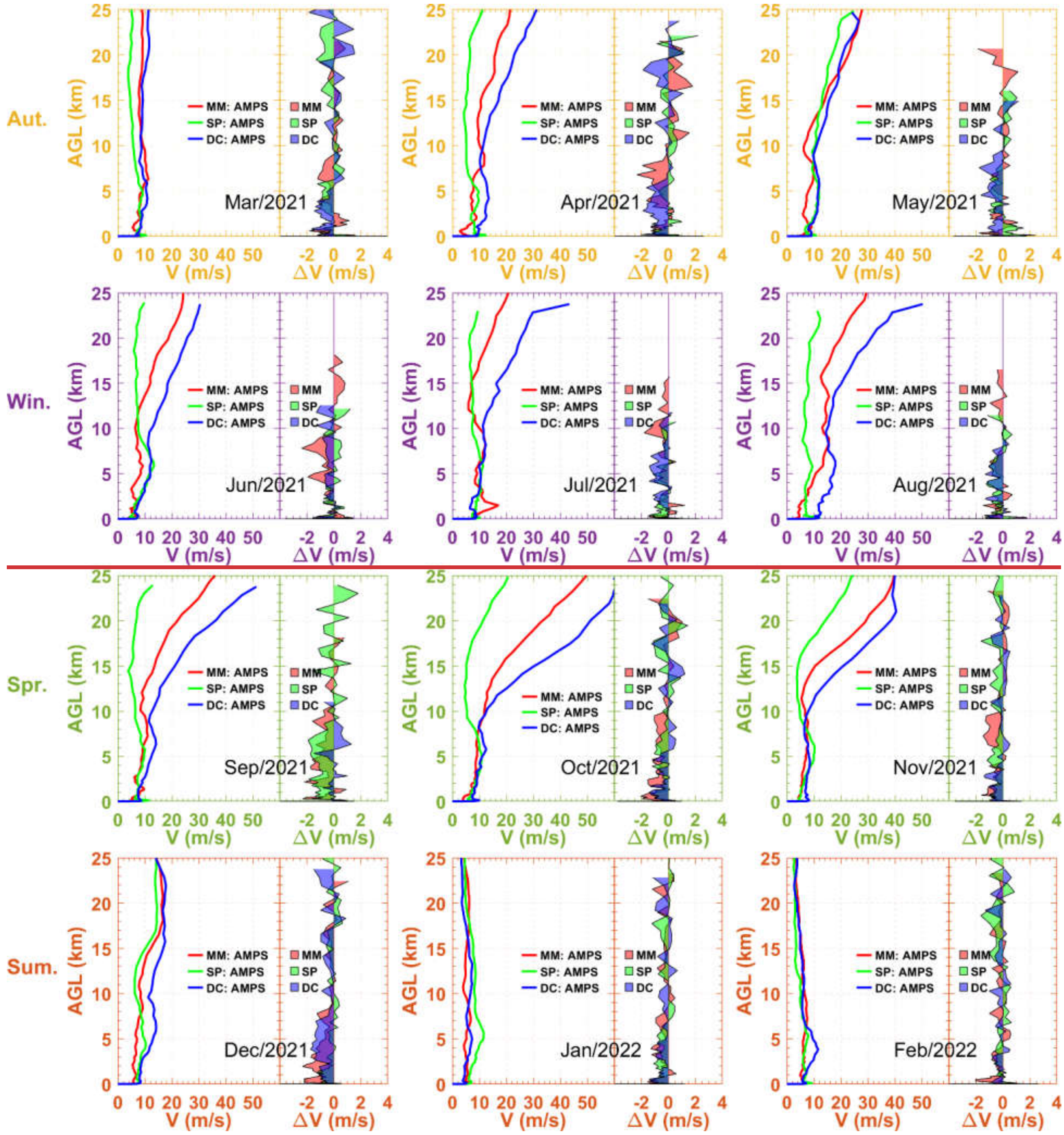


~~Figure 3. As in~~ Fig~~ 2, but for wind speed (=), and .~~

~~Fig~~. 2 shows that the ~~forecasted temperature profiles of SP and DC in the first 5 km are similar, 15-20 K colder than the MM. The median difference in the temperature~~median difference for $\theta$ is of the order of 1 K in the ~~high part of~~ first 5 km (except for the atmosphere ~~(see filled areas in Fig. 2). However,~~layer in proximity to the ground~~, the median difference becomes more significant, especially for winter ,~~). Above 5 km, the AMPS has obviously underestimated the $\theta$ at ~~more than 4 K near~~MM, while the ~~ground~~forecasts at SP~~.~~

~~Fig.~~ and DC are closer to measurements. Fig. 3 shows that the ~~forecasted~~measured wind speed profiles ~~of MM and DC~~ above 10 km at MM and DC are stronger during spring, indicating the occurrence of the Antarctic polar vortex (Boville et al., 1988). However, the change in wind speed above SP is not that obvious, because the Antarctic vortex is roughly pole-~~centred~~centered

(Karpetchko et al., 2005). From the filled areas in Fig. 3, the AMPS forecasts appear consistent with the measurements, as the median difference in wind speed is generally ~1 m $s^{-1}$ and has barely exceeded 2 m $s^{-1}$, whether the wind is strong or weak. In the first 10 km, most $\Delta V$ at the three sites are less than 0, suggesting that the AMPS underestimated the wind speed. Table 2 shows the statistical evaluations of $\theta$ and $V$ forecasted by the AMPS. It seems the AMPS can well capture the trend of $\theta$ and $V$ as the correlation coefficient ( $R_{xy}$ ~~In addition, slightly smaller median differences were displayed around 10 km AGL (e.g. September and December, shown in Fig. 3), and the forecasted wind speed also became slightly smaller at that height~~) are all larger than 0.84.

~~In summary, the AMPS almost well forecasted the temperature and wind speed. Nevertheless, it should be noted that both the measurement accuracy and position of radiosoundings may be affected by their flight, and the difference may be smaller when compared with a fixed measuring instrument, such as the Automatic Weather Station . In other words, the functional performance of the AMPS may be better than the results shown in Figs. 2 and 3.~~

## 4.2 Richardson number

### 4.2.1 ~~Monthly statistical~~Statistical analysis

To evaluate the performance of ~~the~~ AMPS in forecasting ~~atmospheric stability or instability~~the possibility of triggering turbulence over the Antarctic continent, the $Ri$ ~~forecasted by~~ estimations between AMPS forecasts and ~~measured by~~ radiosoundings will be ~~provided~~compared. The calculated value of $Ri$ depends on the vertical resolution of meteorological parameters (Troen and Mahrt, 1986; Holtslag et al., 1990). Thus, the meteorological parameters from the radiosoundings and AMPS forecasts ~~and radiosoundings~~ were interpolated into the same height series (as mentioned in Sect. 4.1) to calculate $Ri$. Where $\partial\theta/\partial z$ and $(\partial u/\partial z)^2 + (\partial v/\partial z)^2$ ~~.~~

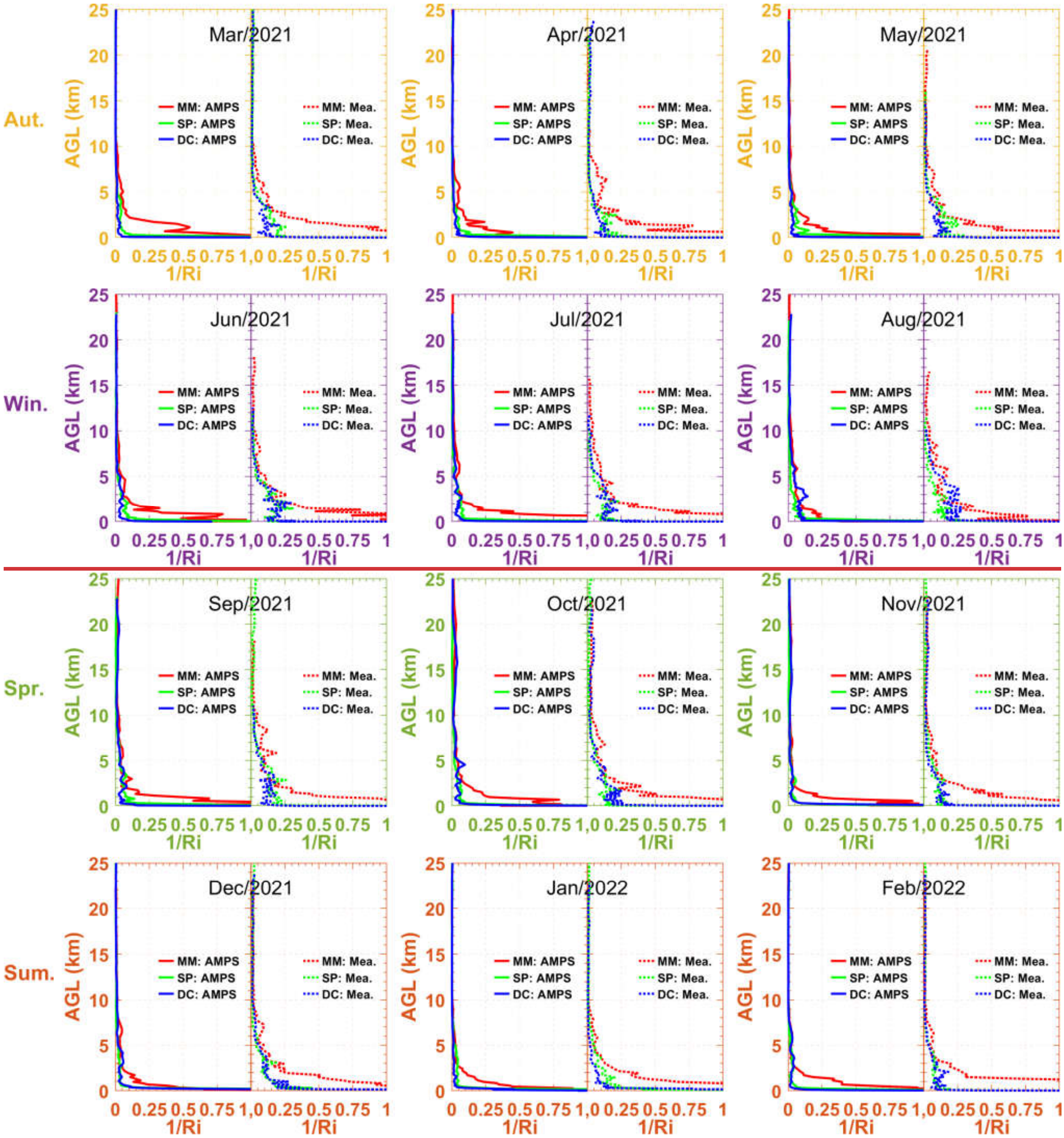


Figure 4. The monthly median _for calculating $Ri$ forecasted by the AMPS (solid lines) and measured by radiosoundings (dashed lines).

The NCL (NCAR Command Language) can compute from the original WRF outputs, using an NCL function called "rigrad_bruntv_atm" (). The NCL (see Eq. (1)) were both computed using a centered finite difference operation, as we found that centered difference performed better than forward difference and backward difference (not shown), i.e., better consistency of $Ri$ (not shown) agrees very well with the results obtained using interpolation (i.e. interpolating the hybrid vertical coordinate to the same height series for each site). between the radiosoundings and AMPS forecasts can be achieved using centered difference.

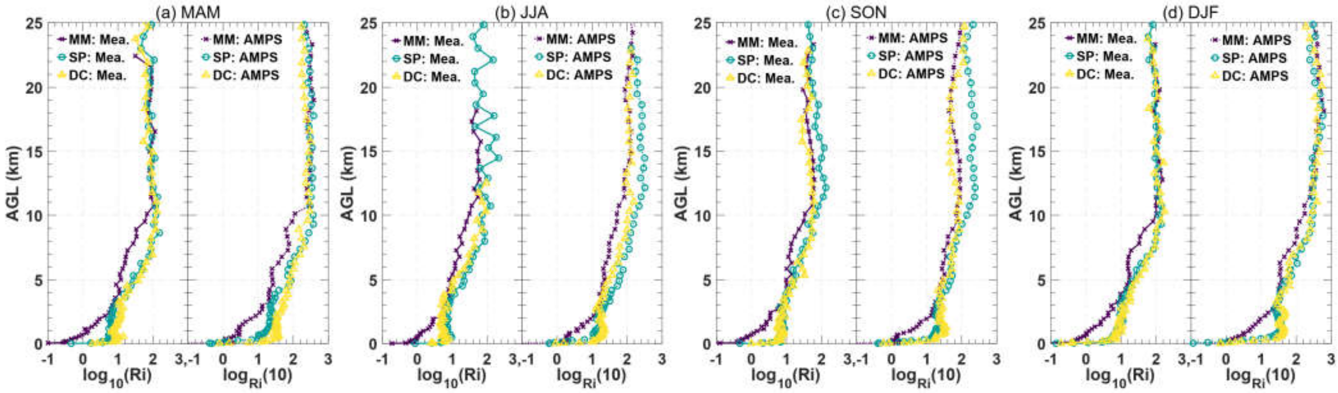


Figure 4. The seasonal median of $\log_{10}(Ri)$ ~~monthly~~ estimated by the radiosonde measurements (solid lines) and the AMPS forecasts (dashed lines).

The seasonal median profiles of $\log_{10}(Ri)$ from the ~~AMPS and~~ radiosoundings and AMPS forecasts are shown in Fig. 4. However, the median differences are not ~~similar to those of~~presented like the $\theta$~~previous temperature~~ and $V$ ~~wind speed.~~. This is because, the $Ri$ value ~~of~~ can ~~oscillate~~vary massively (by two or more orders of magnitude) in the atmosphere, and a precise quantification seems less plausible. Considering this, we initially intended to examine whether AMPS can reconstruct an accurate shape of $\log_{10}(Ri)$ ~~Nevertheless, the AMPS-forecasted~~ profile (while median difference is not suitable for this purpose), and the results from radiosoundings and AMPS forecasts are both presented. Nevertheless, the model bias is by all means of great significance, and it will be discussed later (see Table 2, and Fig. 6). In Fig. 4, one can see that the AMPS-forecasted $Ri$ can identify that the atmosphere above MM tends to be more ~~unstable (or~~ turbulent~~,~~ ( $Ri$ is ~~large~~smaller) than SP and DC~~, per the measurements from radiosoundings. In addition, in~~. In the vertical height direction, the AMPS forecasts can roughly capture the height that can easily trigger turbulence. ~~On the one hand~~For example, one can observe that the $Ri$ from radiosoundings and AMPS forecasts ~~and radiosoundings~~ both show ~~large~~small values very close to the ground at ~~Dome C~~DC and the ~~South Pole~~SP, which is per the fact that strong atmospheric turbulence is concentrated within the surface layer above the high plateau (Marks et al., 1999; Agabi et al., 2006)~~.~~. A very calm atmosphere ( $Ri$ is ~~small~~large) at high altitudes ~~was~~is also consistent with the results given by Travouillon et al. (2003), Aristidi et al. (2005), Trinquet et al. (2008) and Vernin et al. (2009). On the other hand, the AMPS can reconstruct the near-ground "convex-concave–convex" (hereafter "C-C-C") shaped $\log_{10}(Ri)$ profiles indicated by ~~, and . On the other hand, in a more detailed comparison, for example, in March 2021, both forecasts and~~ the radiosonde measurements (see more details in Fig. 5). In terms of time, the AMPS can forecast that the free-atmosphere $Ri$ ~~show that profiles are inclined to the y-axis at ~10 km AGL, and in December 2021, the AMPS forecasts are able to capture a small bump of that occurred at around 7 km AGL.~~ decreased during spring (SON), this decrease is obvious for MM and DC (where the wind speed are significantly stronger during SON, as in Fig. 3).

~~Some researchers are afraid to conduct quantitative~~Quantitative analysis for the ~~model~~ estimated $Ri$ from the numerical models was generally missed as it always varies dramatically (e.g., Hagelin et al., 2008, who focused on the qualitative analysis). Nevertheless, quantitative analysis has been tried in this study since that can give a precise evaluation of the forecast ability of AMPS. Then, the $R_{xy}$ ~~correlation coefficient ()~~,, mean bias ( $Bias$ ; AMPS-~~radiosoundings~~radiosonde), and root mean square error ( $RMSE$ ) are calculated~~. Here,~~ using the combined data of all profiles for each season. Where the time difference between radiosoundings and AMPS forecasts ~~and radiosoundings, with lesser~~was limited to less than 1.5 hours~~, is used. This is the same as the meteorological parameters mentioned in Sect. 4.1. Besides, all profile data meeting the time constraints are also limited to a value range of (0, 1), which is the same as the x-axis in Fig. 4.~~. Finally, the ~~monthly~~seasonal values of the three statistical operators are ~~obtained~~calculated, as ~~shown~~listed in ~~Fig. 5~~Table 2. However, we want to ~~emphasise~~emphasize that one should focus on the value of $R_{xy}$ that reflects the tendency, instead of $Bias$ and $RMSE$, as a precise quantification remains in doubt (Hagelin et al., 2008). The mean values of $R_{xy}$ ~~the combined 12 monthly in Fig. 5a for MM, SP, and DC, are 0.71, 0.66, and 0.68, respectively. This suggests that the AMPS-forecasted can identify the main characteristics of atmospheric turbulence over the Antarctic continent in terms of space and time. In terms of time, one can observe larger during warm seasons (e.g. Autumn from March 2021 to May 2021 and summer from December 2021 to February 2022). In sum, the AMPS seems to perform better when more measurements can be obtained. As we know, more field experiments could be conducted at the coast (MM) in the space dimension (one can reach the coast easier than the internal Antarctic Plateau) and during warm seasons (e.g., summer) in the time dimension (the cold is much harder to endure in winter than it is in summer).~~

~~Fig. 5b shows that is underestimated every season, and the mean values of the 12 monthly~~ for MM, SP, and DC over four seasons are 0.71, 0.59, and 0.53, respectively. The highest $R_{xy}$ is at MM for DJF (0.77) and the lowest is at DC for JJA (0.45). We found that these two cases correspond to the most unstable and stable atmospheric conditions, their median $[\theta_{1000\,\mathrm{m}}-\theta_{0\,\mathrm{m}}]/[1000\,\mathrm{m}-0\,\mathrm{m}]$ ~~are -0.097, -0.031, and -0.071~~ equal to 0.0038 and 0.0721, respectively. This suggests that the AMPS can better capture the trend of $\log_{10}(Ri)$ ~~This may be because the model results were generally smoother than the measurements. The atmosphere is favourable for the occurrence of turbulence ( is large) under rapidly changing meteorological parameters. Fig. 5c shows that at MM is the largest, which may be due to the~~ at a relatively unstable atmosphere~~ above it and could fluctuate massively.~~

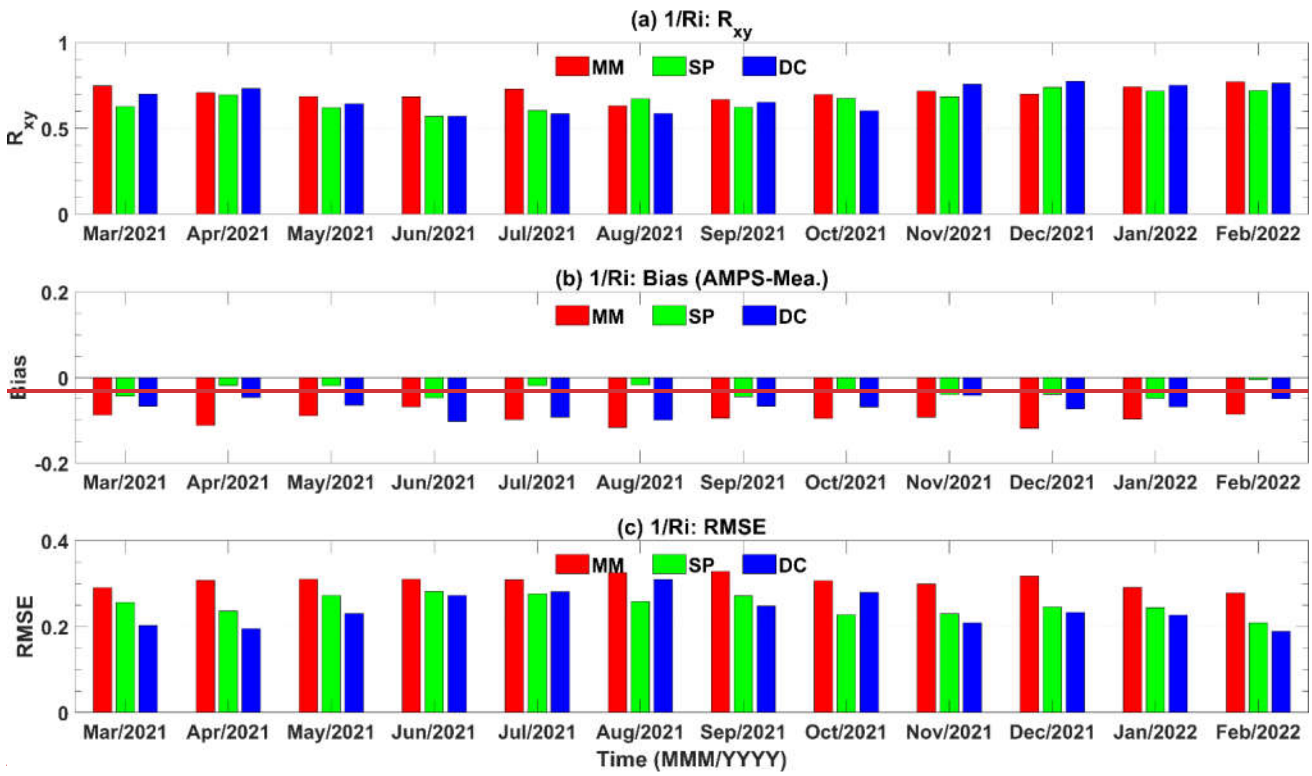


~~Figure 5. The monthly statistics for three sites.~~

### ~~4.2.2 Vertical distribution~~

~~To further investigate the difference between the radiosounding and model results, the vertical distributions of the whole year~~. However, the *Bias* ~~at the three sites are shown in Fig. 6. The reason~~ is the largest (0.47) in the most unstable case. This is because the AMPS overestimated the potential temperature gradient under an unstable atmosphere (see Fig. 6a, which will be discussed later). For the stable atmosphere, the lowest $R_{xy}$ for $\log_{10}(Ri)$ ~~using (not , as presented in Sect. 4.2.1) is~~ seems to be consistent with the fact that model errors increase with increasing stability (Nigro et al., 2017)~~we find that the distribution will be more linear at the same height. Fig. 6a shows that the data points are distributed mainly over the diagonal line between the measurements and the forecasts, this suggests the AMPS can make a better forecast at McMurdo than at the South Pole (Fig. 6b) and Dome C (Fig. 6c).~~.

Table 2 also shows an interesting result: the $R_{xy}$ of $\log_{10}(Ri)$ is higher when the *RMSE* of $\theta$ and $V$ are smaller. Moreover, Hines et al. (2019) showed that using the Morrison microphysics scheme in the numerical model resulted in a smaller *RMSE* for temperature and wind, than the default scheme (WSM5C) in AMPS. Therefore, we may conclude that replacing WSM5C with Morrison could improve the AMPS-forecasted $\log_{10}(Ri)$. In other words, using Morrison may lead to higher $R_{xy}$ for $\log_{10}(Ri)$, as it simulates dynamic stability with less variability (the *RMSE* for temperature and wind could be smaller). On the other hand, larger *RMSE* for $\theta$ and $V$ are mainly found during cold months (JJA, SON), indicating that winter dynamic stability is more variable (similar to Bromwich et al., 2013).

Table 2 summarises that the $\log_{10}(Ri)$ was overestimated by the AMPS at each site for every season (all *Bias* are positive). This may be due to some local-scale dynamics not being represented properly (see Fig. 6, which will be discussed later). From another perspective, the model results were generally smoother than the measurements, and the atmosphere is less favorable for the occurrence of turbulence under slowly changing meteorological parameters, then the AMPS-forecasted $Ri$ could be larger.

Table 2. Statistical evaluations of the potential temperature ($\theta$), wind speed ($V$), and logarithmic Richardson number ($\log_{10}(Ri)$) forecasted by the AMPS when compared with the results from radiosonde measurements.

| | McMurdo | | | | South Pole | | | | Dome C | | | |
|---|---|---|---|---|---|---|---|---|---|---|---|---|
| Season | MAM | JJA | SON | DJF | MAM | JJA | SON | DJF | MAM | JJA | SON | DJF |
| $\theta$: $R_{xy}$ | 0.99 | 0.99 | 0.99 | 0.99 | 0.99 | 0.99 | 0.99 | 0.99 | 0.99 | 0.99 | 0.99 | 0.99 |
| $\theta$: *Bias* | -0.32 | -0.61 | -0.10 | -0.23 | -1.30 | -1.41 | -1.45 | -0.94 | -0.74 | -0.58 | -0.25 | 0.19 |
| $\theta$: *RMSE* | 1.82 | 1.91 | 1.78 | 1.56 | 2.65 | 2.88 | 3.48 | 2.43 | 4.28 | 2.22 | 2.38 | 1.76 |
| $V$: $R_{xy}$ | 0.85 | 0.89 | 0.95 | 0.90 | 0.86 | 0.84 | 0.89 | 0.90 | 0.92 | 0.92 | 0.97 | 0.95 |
| $V$: *Bias* | -0.25 | -0.25 | -0.59 | -0.67 | -0.16 | -0.29 | -0.64 | -0.40 | -0.62 | -0.43 | -0.24 | -0.50 |
| $V$: *RMSE* | 3.16 | 3.63 | 3.23 | 2.81 | 2.52 | 2.90 | 2.69 | 2.37 | 2.50 | 2.94 | 2.69 | 1.89 |
| $\log_{10}(Ri)$: $R_{xy}$ | 0.75 | 0.65 | 0.68 | 0.77 | 0.61 | 0.50 | 0.56 | 0.70 | 0.51 | 0.45 | 0.50 | 0.66 |
| $\log_{10}(Ri)$: *Bias* | 0.41 | 0.32 | 0.33 | 0.47 | 0.36 | 0.23 | 0.29 | 0.35 | 0.45 | 0.39 | 0.30 | 0.46 |
| $\log_{10}(Ri)$: *RMSE* | 0.90 | 0.86 | 0.88 | 0.93 | 0.90 | 0.84 | 0.85 | 0.90 | 0.93 | 0.86 | 0.81 | 0.91 |

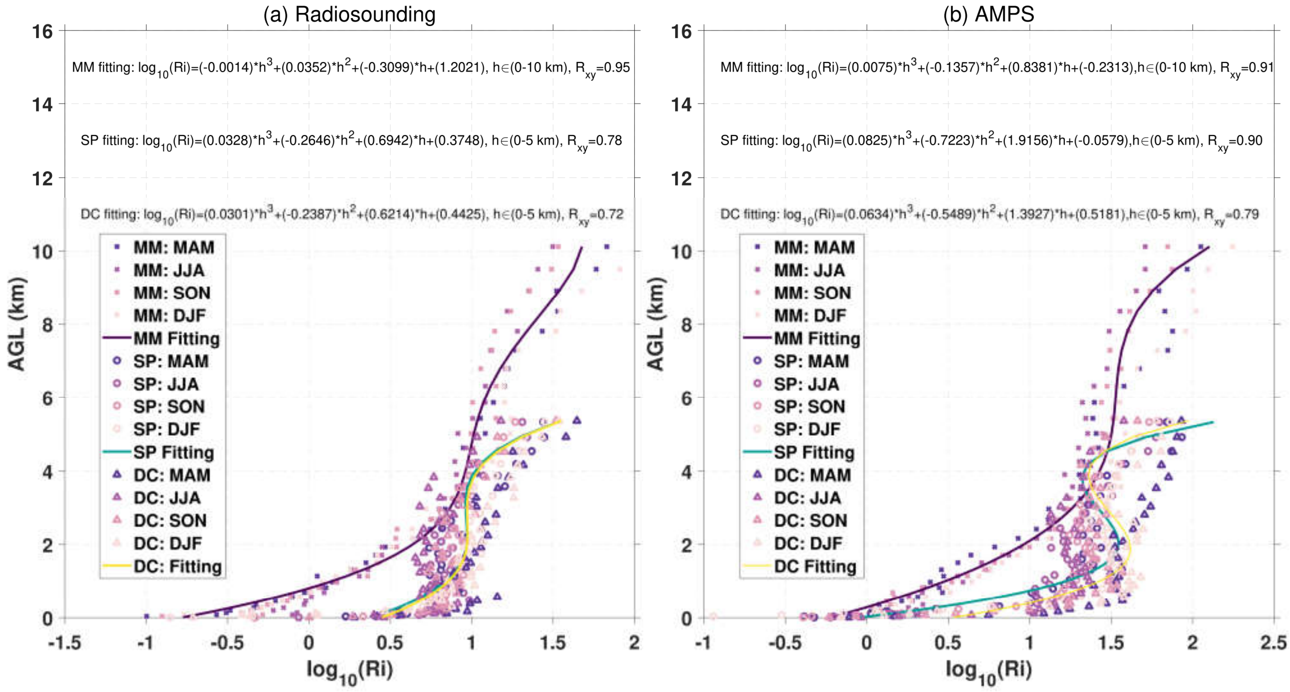


Figure 5. The polynomial curve fitting of near-ground median profiles of $\log_{10}(Ri)$ from Fig. 4; (a) the $\log_{10}(Ri)$ was estimated by the radiosonde measurements, (b) the $\log_{10}(Ri)$ was estimated by the AMPS forecasts.

The near-ground atmosphere in Antarctica is an important turbulence source, then an analytical function for $\log_{10}(Ri)$ profiles near the ground was fitted to better contextualize the results (as shown in Fig. 5). Fig. 5 shows that the near-ground $\log_{10}(Ri)$ profiles are the "C-C-C" shape. The "concave" structure in the "C-C-C" shape could be attributed by the near-ground jet stream (Mihalikova et al., 2012). A cubic polynomial function was used (see the upper part of the plots in Fig. 5) instead of a logarithmic function, because the "C-C-C" shape seems hard for logarithmic function fitting. Moreover, each fitted curve used all four-seasons data points in Fig. 4, as the seasonal variation are not too significant. Nevertheless, one can see more details about the temporal variation of $\log_{10}(Ri)$ near the ground in Sect. 4.2.3.

Fig. 6 shows the AMPS performance under different potential temperature gradient ( $G=\partial\theta/\partial z$ ) and wind shear ( $S=\left[\left(\partial u/\partial z\right)^2+\left(\partial v/\partial z\right)^2\right]^{1/2}$ ). The statistical results presented in Fig. 6 were counted based on all the collected data points at the three sites (MM, SP, and DC) for an entire year. One can see that the $Ri$ was overestimated by the AMPS at an unstable atmosphere (see light blue bin in Fig. 6a), where the AMPS has overestimated the potential temperature gradient (i.e. $\Delta G>0$ ). But for strong temperature inversion (see dark red bin in Fig. 6a), the AMPS has underestimated the $G$ and $Ri$ . As for strong wind shear conditions (see dark red bin in Fig. 6b), when the $Ri$ is small (basically corresponding to a near-surface layer with a high probability of triggering strong turbulence, as in Fig. 4), the AMPS has underestimated the intensity of wind shear ( $\Delta S<0$ ). This may be caused by the AMPS has underestimated the wind speed near the ground (as in Fig. 3). In sum, if the model aims for a more accurate forecast of $Ri$ , the biases under these atmospheric conditions need to be corrected.

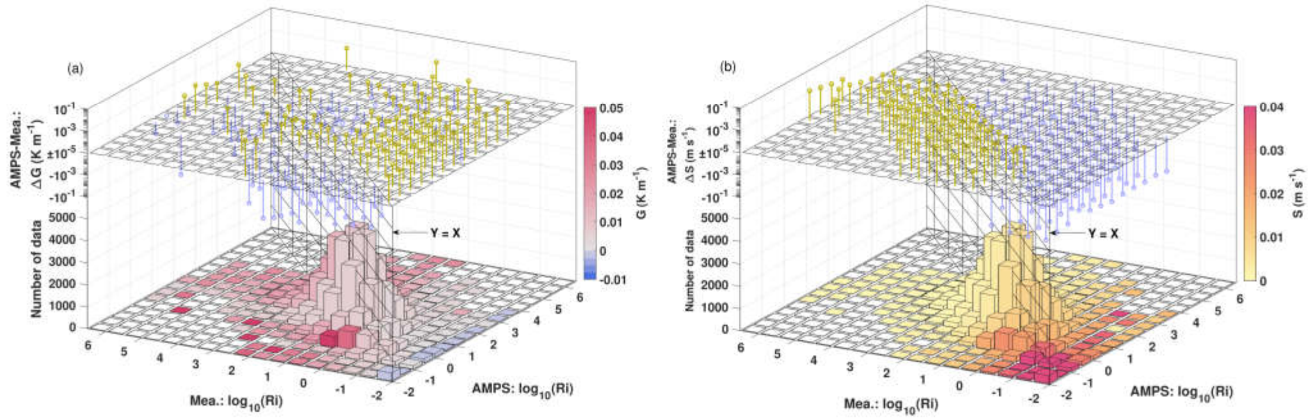


Figure 6. Performance of the AMPS under different atmospheric conditions. (a) and (b) are respectively the case of potential temperature gradient ( $G=\partial\theta/\partial z$ ) and wind shear ( $S=\left[\left(\partial u/\partial z\right)^2+\left(\partial v/\partial z\right)^2\right]^{1/2}$ ). $G$ (color of the bin in (a)), $S$ (color of the bin in (b)), $\Delta G$ (stem above the bin in (a)) and $\Delta S$ (stem above the bin in (b)) are presented using the median value for each 0.5×0.5 bin of $\log_{10}\left(Ri\right)$

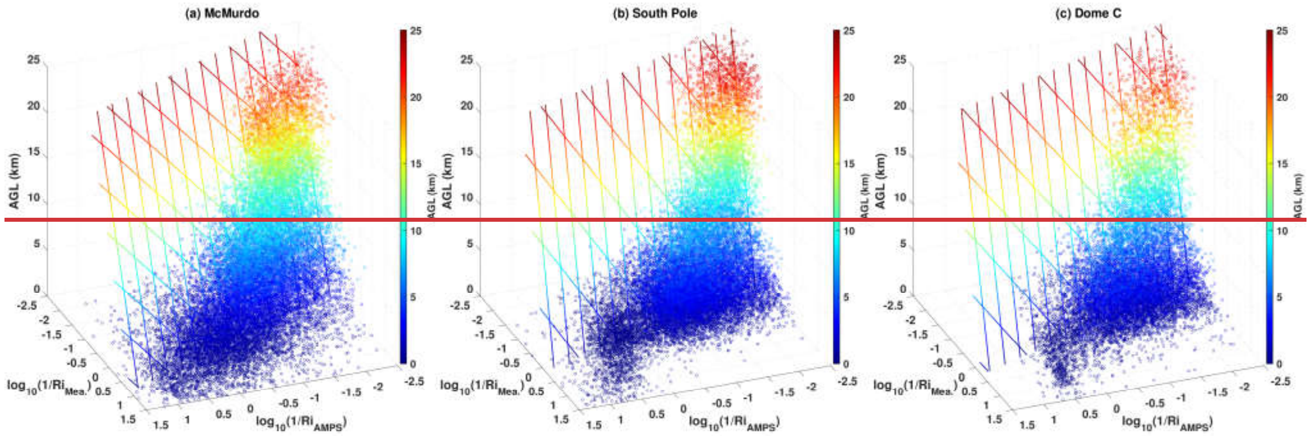


Figure 6. the vertical distributions of whole-year from the AMPS and the measurements at McMurdo (a), the South Pole (b), and Dome C (c). The coloured grid lines represent the fitted planes using the presented data points.

We assume that the difference between the measurements and model results was correlated with height (or AGL, here indicated by ), and a simple model to improve the AMPS forecasted by considering (km) is given by the following linear equation:

.

The three undetermined coefficients (, , and ) can be determined using a linear fitting by the measurements, (i.e. will be replaced with for fitting).

Table 2. The fitted model for improving the AMPS-forecasted .

| Site | Model: $\log_{10}\left(1/Ri_{\text{ImpAMPS}}\right)=C_1+C_2\cdot\log_{10}\left(1/Ri_{\text{AMPS}}\right)+C_3\cdot H$ | $R_{xy}$ (Before)[a] | $R_{xy}$ (After)[b] |
|---|---|---|---|
| McMurdo | $\log_{10}\left(1/Ri_{\text{ImpAMPS}}\right)=0.1222+0.4826\cdot\log_{10}\left(1/Ri_{\text{AMPS}}\right)-0.0660\cdot H$ | 0.7215 | 0.7691 |

| | | | |
|---|---|---|---|
| South Pole | $\log_{10}\left(1/Ri_{\mathrm{ImpAMPS}}\right) = -0.4414 + 0.3827\cdot\log_{10}\left(1/Ri_{\mathrm{AMPS}}\right) - 0.0387\cdot H$ | 0.6009 | 0.6391 |
| Dome C | $\log_{10}\left(1/Ri_{\mathrm{ImpAMPS}}\right) = -0.3596 + 0.3977\cdot\log_{10}\left(1/Ri_{\mathrm{AMPS}}\right) - 0.0457\cdot H$ | 0.4730 | 0.5235 |

[a] Correlation coefficient between and (i.e. before using the fitted model).

[b] Correlation coefficient between and (i.e. after using the fitted model).

Table 2 lists the fitted model and its corresponding improvements. The correlation coefficient at all three sites increased after using the fitted model, which means that the fitted model can be used to modify the AMPS forecasts () and obtain an improved result (). Through analysis of the fitted model, one can see the undetermined coefficient is less than 1, we find this is due to the AMPS underestimated when <0; the undetermined coefficient is negative, indicating the negative regulating action for with increasing height.

4.2.3.

### 4.2.2 Vertical cross-section

The results are given in Sect. 4.2.1 that showsshow the AMPS can forecast the main tendency of $\log_{10}(Ri)$. Then, we consider that it is worth a try to use the AMPS-forecasted $\log_{10}(Ri)$ to comprehend the characteristics of atmospheric turbulence in Antarctica. The results of the AMPS-forecasted $\log_{10}(Ri)$. The analysis of was done was presented through interpolation of the AMPS grid 2 field withat two vertical cross-sections, which provides us with a broader perspective on the probability of turbulence triggered in four-dimensional space-time. One vertical cross-section is interpolated through two specified points (the South PoleSP and Dome C),DC, and another is through Dome ADA and McMurdo (MM, as shown in Fig. 7).. The corresponding AMPS forecasts are shown in FigFigs. 8 and 9, respectively.

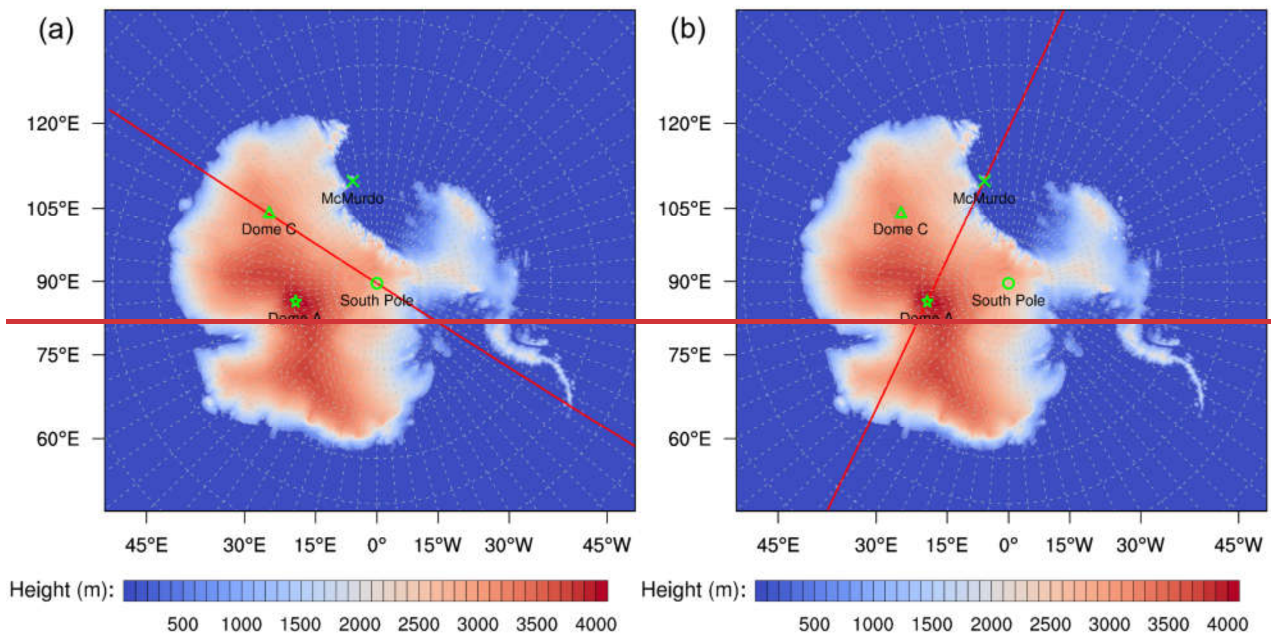

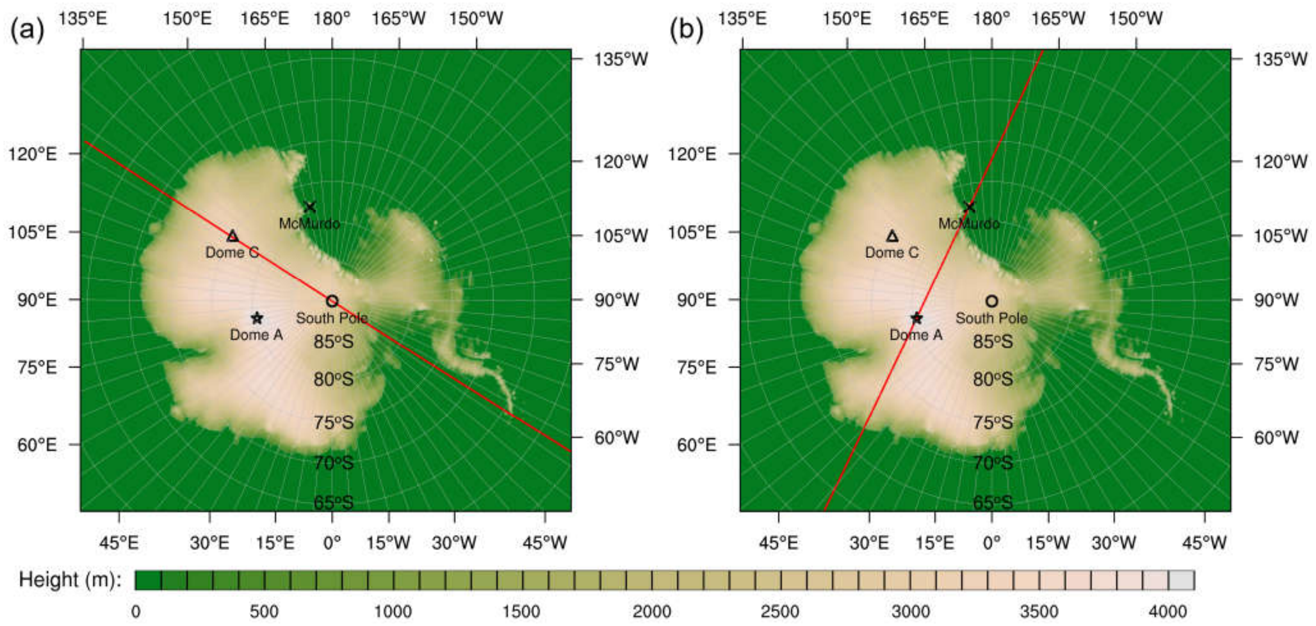


Figure 7. Two lines (marked by red lines) are used to create vertical cross-sections. (a) a line through ~~Dome C~~DC and the ~~South Pole~~SP, (b) a line through ~~Dome A~~DA and ~~McMurdo~~MM. The ~~colour~~color scale indicates the terrain height (m~~).~~

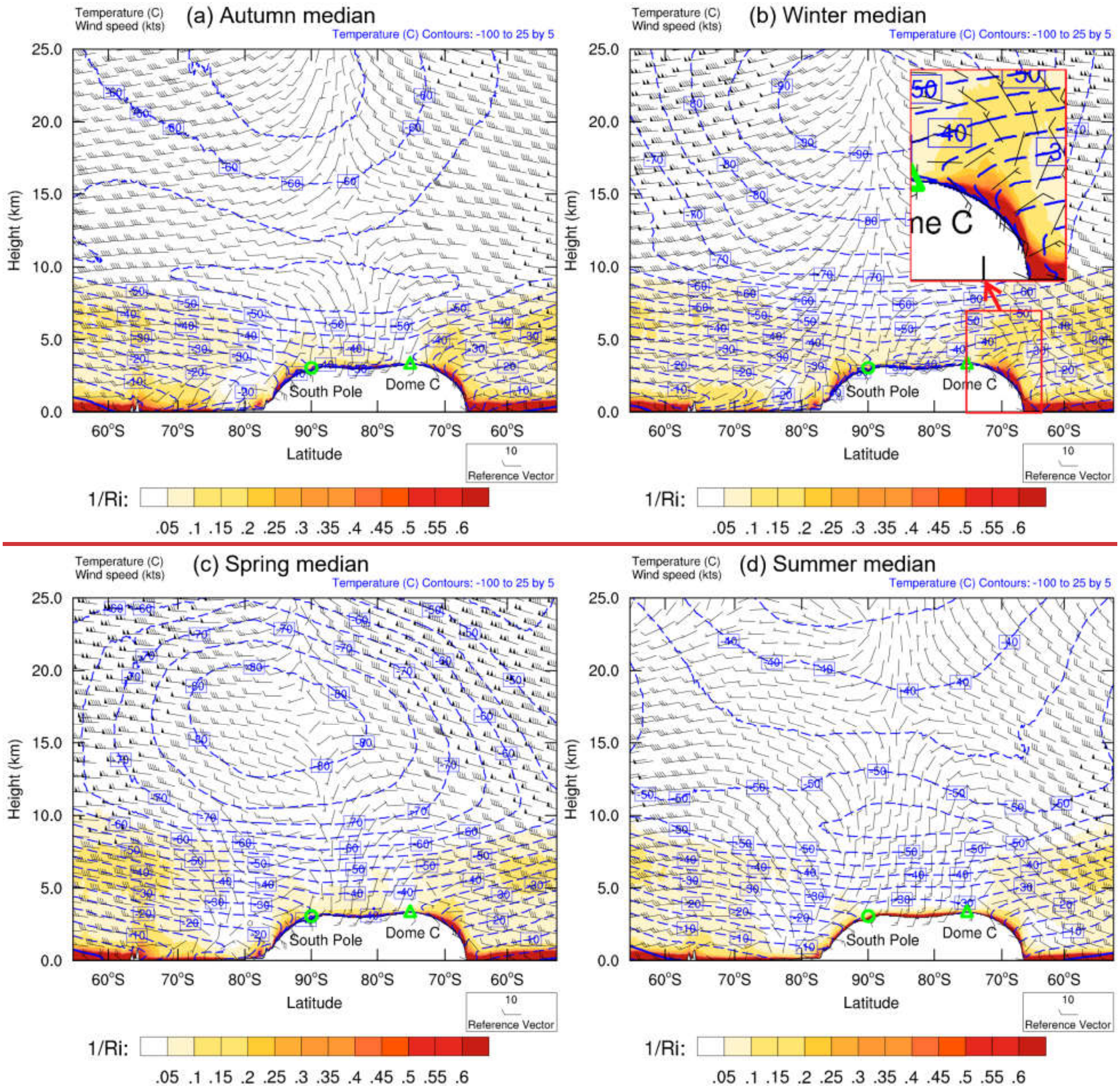


~~Figure 8. Median vertical cross-section of temperature, wind speed, and along the red line through the South Pole and Dome C (shown in Fig. 7a). The height (km) on the y-axis represents the elevation above sea level. The seasonal median for autumn: March 2021 to May 2021 (a), winter: June 2021 to August 2021 (b), spring: September 2021 to November 2021 (c), and summer: December 2021 to February 2022 (d)~~), where terrain fields are ~~given. The reference vector is 10 kts (~5.2 m s$^{-1}$) for the wind barb. Winds are depicted as blowing~~generated from the ~~direction the flags are facing (earth coordinates), e.g., the reference vector represents wind blowing from the west.~~RAMP2 data set (https://nsidc.org/data/nsidc-0082/versions/2).

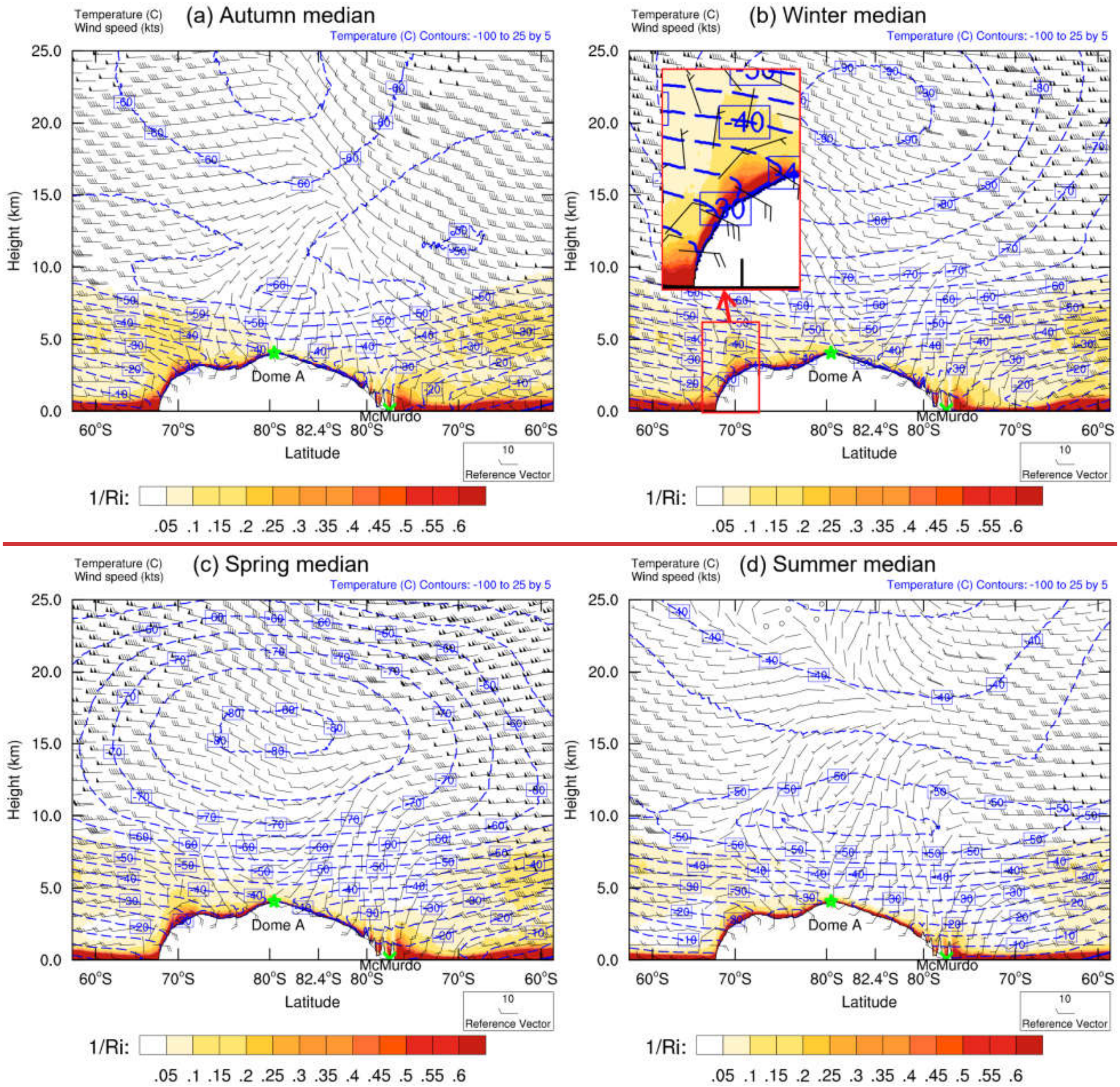


~~Figure 9. As in Fig. 8, but for the vertical section along the red line through Dome A and McMurdo (shown in Fig. 7b).~~

Figs. 8 and 9 show the seasonal median of the AMPS forecasts. The temperature and wind speed were lower above the Antarctic Plateau than over the ocean. In the polar winter~~,~~ (JJA), the temperature contours are dense near the ground above the interior Plateau, representing a strong surface-layer temperature inversion (such inversion has been observed by Yagüe et al., 2001; Argentini et al., 2013; Hu et al., 2019). The surface-layer wind speeds increase from the summit to the escarpment region (caused by the well-known katabatic wind over the surface slope area in Antarctica) and then decrease toward the coast, which is consistent with previous measurements (Ma et al., 2010; Rinke et al., 2012). The $Ri$ is obviously larger above the summits (e.g. DA and DC), suggesting the $PBLH$ could be thin, this agrees with the results from Swain and Gallée (2006); Bonner et al. (2010); and Aristidi et al. (2015)~~. The depths of large near the ground are thinner near the summits (e.g. Dome A and Dome C) of the Antarctic Plateau . Notably, a thick depth of large (which could be considered thick and will be discussed later) occurred near the escarpment region from the side of the internal plateau, as clearly shown during winter (see the enlarged drawings in~~

~~Figs. 8 and 9). Owing to the forecast ability of AMPS in vertical space, one can see that this high is caused by the wind shear, where the wind direction is southeast within the surface layer and changes to the northwest at ~ 5 km AGL.~~ .

The results of $Ri$ distribution from the AMPS outputs provided us with valuable insights into the atmospheric turbulence in the Antarctic region (while using the radiosonde measurements is hard to do so). Here, we attempt to relate the features of atmospheric turbulence to some large-scale phenomena or local-scale dynamics over the Antarctic plateau and the ocean surrounding it: the shear-induced turbulence (katabatic winds, polar vortices), convection (cloud cooling, boundary layer convection), temperature inversion, and the wave-induced turbulence (orographic gravity waves, trapped lee waves, inertia-gravity waves). Table 3 lists their possible functional areas that are marked in Figs. 8 and 9. This is dedicated to qualitatively evaluating the AMPS outputs and investigating the underlying physical processes of triggering atmospheric turbulence.

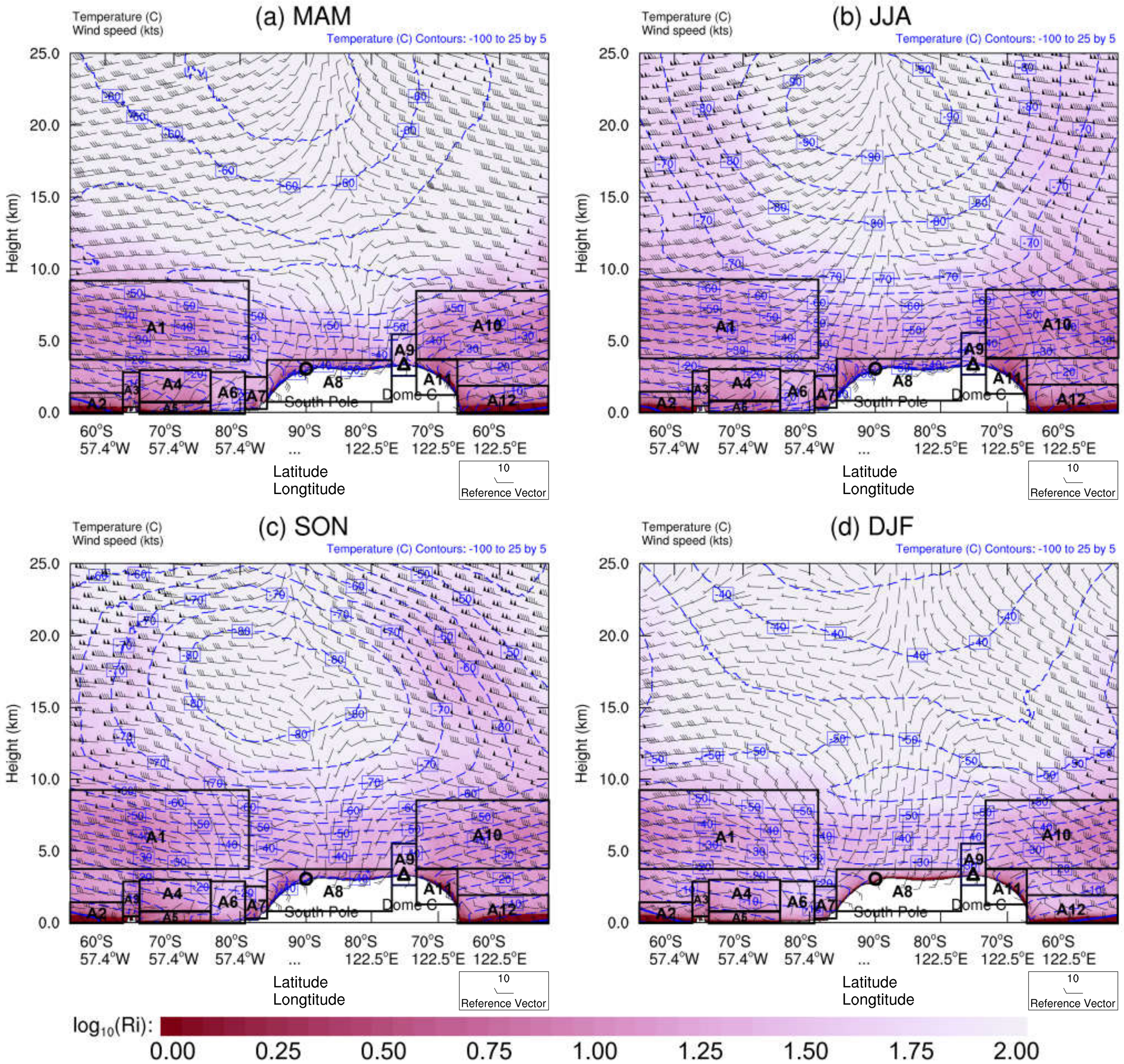


Figure 8. The seasonal median of temperature (instead of $\theta$), wind speed, and $\log_{10}(Ri)$ along the vertical cross-section through the South Pole (black circle) and Dome C (black triangle), as shown by the red line in Fig. 7a. The height (km) on the y-axis

represents the elevation above sea level. The $AX$ in each plot are used to mark the possible functional areas of some atmospheric activities (as listed in Table 3).

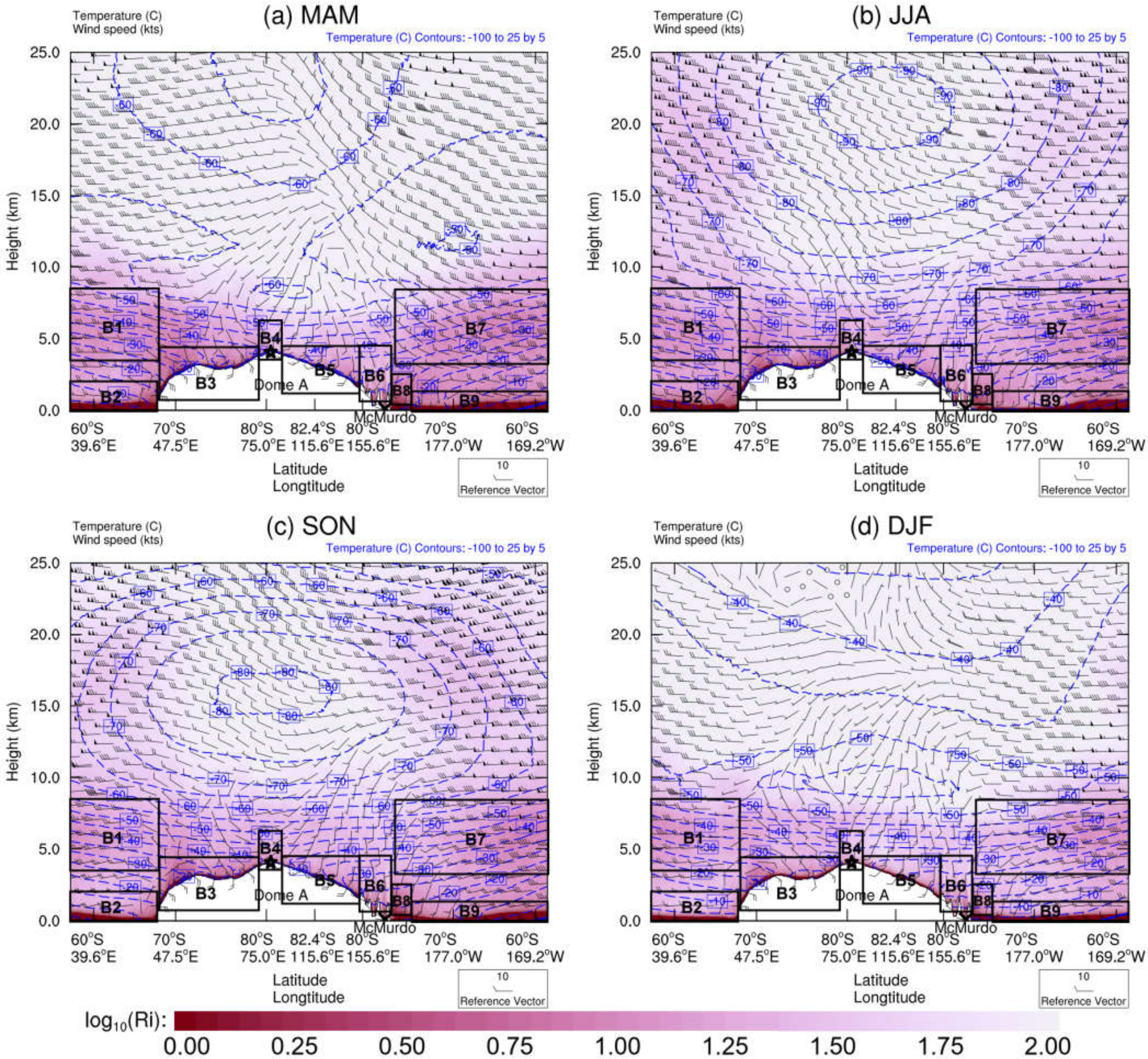


Figure 9. As in Fig. 8, but for the vertical cross-section through Dome A (black star) and McMurdo (black cross), as shown by the red line in Fig. 7b.

As a result of katabatic winds (Rinke et al., 2012), the near-surface wind speeds increase from the interior plateau to the steep slope (Figs. 8 and 9), which is driven by gravity. Strong winds can lead to strong wind shear and increased levels of mechanical turbulence (e.g., Huang et al., 2021; Solanki et al., 2022), as one can see the surface layer with small $Ri$ at the escarpment region (see A8 and A11 areas in Fig. 8, B3 and B5 areas in Fig. 9). Where the regions between the SP and DC (in A8 area) are also located on the slope (see Fig. 7a) and show a relatively small $Ri$ near the ground.

A strong polar vortex implies that the zonal winds are intense, and atmospheric turbulence is more prone to occur. The Antarctic polar vortex reaches its maximum intensity in the winter-spring season (Zuev and Savelieva, 2019a), which corresponds to the relatively turbulent free atmosphere with low $Ri$ values over the ocean during JJA and SON (see Figs. 8 and 9). Moreover, the strongest zonal winds are located over the ocean (Zuev and Savelieva, 2019b), the interaction between the zonal wind and the ocean surface may generate wind shear and facilitate the development of turbulence (see areas A2 and A12 in Fig. 8, B2 and B9 in Fig. 9).

Cloud cooling refers to two kinds of cooling-induced turbulence in this study: Cloud Top Cooling (CTC) and Below Cloud-base Turbulence (BCT). The CTC is contributed by radiative cooling, which could be one of the driving mechanisms of the mixed-layer turbulence (Deardorff, 1976). The BCT usually occurs below the bases of midlevel clouds accompanied by precipitation that does not reach the ground, cooling by evaporation or sublimation seems to contribute to the turbulence (Kudo, 2013; Kantha et al., 2019). In sum, regions with clouds may advance the development of turbulence. The cloud fraction observed by satellite lidar is higher above the ocean than the Antarctic plateau (Spinhirne et al., 2005; Saunders et al., 2009). Thus, cloud may benfit small $\log_{10}(Ri)$ above the ocean (A1 and A10 areas in Fig. 8, plus the B1 and B7 areas in Fig. 9).

Boundary layer convection is generated by forcing from the ground, solar heating of the ground during sunny days causes thermals of warmer air to rise and convection will form (He et al., 2020), then the turbulence could be developed forced by buoyancy (Verma et al., 2017). The albedo of fresh snow over sea ice is very high, while that for open water is relatively small (Hines et al., 2015). Thus, solar heating will be much more stand out over open water and lead to the thermal convection boom. This can be used to reasonably explain the results in Fig. 8, that the $Ri$ over ocean (A2 area) is smaller than over ice shelf (A6 area), and the A5 area can be regarded as a "transition region" (sea ice and open water could both exist) between them with an intermediate value of $Ri$.

Table 3. The possible functional areas of some typical large-scale phenomena or local-scale dynamics over the Antarctic plateau and the ocean surrounding it.

| | Possible functional areas | | |
|---|---|---|---|
| Atmospheric activities | Marked areas in Fig. 8 | Marked areas in Fig. 9 | Contribution for triggering turbulence |
| Katabatic winds | A8, A11 | B3, B5 | Positive |
| Polar vortices | A1, A2, A5, A10, A12 | B1, B2, B7, B9 | Positive |
| Cloud cooling | A1, A10 | B1, B7 | Positive |
| Boundary layer convection | A2, A5, A12 | B2, B9 | Positive |
| Temperature inversion | A6, A9 | B4 | Negative |
| Orographic gravity waves | A3 | B6 | Positive |
| Trapped lee waves | A4, A7 | B8 | Positive |
| Inertia-gravity waves | A1, A10 | B1, B7 | Positive |

The strength of the near-ground temperature inversion forecasted by the AMPS increases from the coast to the high interior, and its strength weakens during polar summer, such a phenomenon has also been observed in previous studies (Hudson and Brandt, 2005; Ma et al., 2010). The general increase in temperature-inversion strength was considered to correspond to a less turbulent atmosphere (when the boundary layer is shallower), owing to large stability suppressing turbulence. This corresponds to the larger $Ri$ in the summit area where a stronger temperature inversion occurred (see A9 area in Fig. 8 and B4 area in Fig.

9). There is a similar phenomenon occurred over the Ronne ice shelf (A6 area in Fig. 8), especially for JJA (when the temperature inversion is more obvious). Importantly, it should be noted that it is the range of turbulence (or $PBLH$ ) that would be suppressed by the temperature inversion and the turbulence intensity could be strong within the inversion layer (Petenko et al., 2019). For example, the turbulence above Dome C is mainly concentrated in the first tens of meters above the ground (Aristidi et al., 2015).

The development of Orographic Gravity Wave (OGW) is the interaction between near-surface wind and a mountain barrier (Lv et al., 2021; Zhang et al., 2022a; Zhang et al., 2022b), the OGW breaking could be a source of turbulence. Obviously, OGW can be triggered above the Antarctic Peninsula (A3 area in Fig. 8) and Transantarctic Mountains (B6 area in Fig. 9). But the atmosphere just above the top of the mountain seems to be laminar (e.g., see the larger value of $Ri$ in B6 area), this may be due to that the breaking of the OGW may not happen immediately after being generated above the mountains.

Trapped Lee Waves (TLW) belongs to OGW. Specially, TLW, as its name implies, tends to form on the lee side of mountains and turbulence may be developed in the downstream (Xue et al., 2022). Thus, the small $Ri$ in A4 area in Fig. 8 can be attributed by the TLW forced by the Antarctic Peninsula (see its position in Fig. 7a). It is the same case for B8 area in Fig. 9 (but forced by the Transantarctic Mountains). The katabatic winds could be linked to TLW and result in enhanced turbulence, This could explain the A7 area (Fig. 8) have small $Ri$ on the lee side of the mountain.

Inertia-Gravity Waves (IGW) are influenced by the Coriolis effect (increasing with wind speed), and the frequency of IGW is close to inertial frequency. IGW and Kelvin-Helmholtz instability (which can be characterized by the Richardson number) are generally presumed to be closely linked. At high latitudes, the IGW energy density's maxima occur at around 5 km AGL (Zhang et al., 2022a). This may suggest that the IGW can also be a contributor to the small $Ri$ above the ocean (A1 and A10 areas in Fig. 8, plus the B1 and B7 areas in Fig. 9).

In addition, one can see the temporal evolution of $Ri$ vertical cross-sections for a year from the video supplement (vertical cross-section through the red line shown in Fig. 7a: https://doi.org/10.5446/60761; and Fig. 7b: https://doi.org/10.5446/60760). It shows that the atmospheric conditions are variable, and a significant transition between laminar flow and turbulent flow could occur at any time. Some activities in Antarctica require a non-turbulent atmosphere, such as astronomical observations (Burton, 2010) and aviation safety (Gultepe and Feltz, 2019)atmosphere exhibited strong daily variability. Thus, . Therefore, real-time forecasting is necessary if one wishes to avoid a turbulent atmosphere in Antarctica, instead of counting only on the displayedof the Richardson number is important and helpful, rather than relying solely on the statistical results. Moreover, unstable atmospheres are presented in this study. Furthermore, the video shows that atmospheric turbulence is likely to be triggered over the ocean, moving toward the Antarctic Plateau and becoming stable.weakening. This was likelymay be due to the obstruction of the high plateau, and thewhich creates a calm atmosphere above it behaved calmly.

#### 4.2.43 Richardson number at the planetary boundary layer height

The Richardson number is used to determine the boundary layer height using a critical value, typically 0.25 (Troen and Mahrt, 1986; Holtslag et al., 1990; Pietroni et al., 2012). The . Thus, the critical value (or the value of $Ri$ at the $PBLH$ , $Ri_{PBLH}$ ) is worth studying, which is a significant application for the Richardson number.. In addition, previous studies have suggested that the $Ri_{PBLH}$ Richardson number depends on the vertical resolution of the modeldata (Troen and Mahrt, 1986; Holtslag et al., 1990). ItAs for the resolution of the AMPS grid, it is difficultnecessary to recalculate $Ri_{PBLH}$ define what strong turbulence layer (or atmosphere instability) may appear, whenever a reference standard based on the AMPS outputs, since the value of $Ri_{PBLH}$ is

~~not given.  would thus be~~ a helpful reference ~~standard~~ for judging whether ~~an~~ atmospheric ~~layer~~turbulence is ~~stable~~likely to be suppressed ( $Ri$ ~~<~~$>$ $Ri_{PBLH}$ ) or ~~unstable~~developed ( $Ri$ ~~>~~$<$ $Ri_{PBLH}$ ).

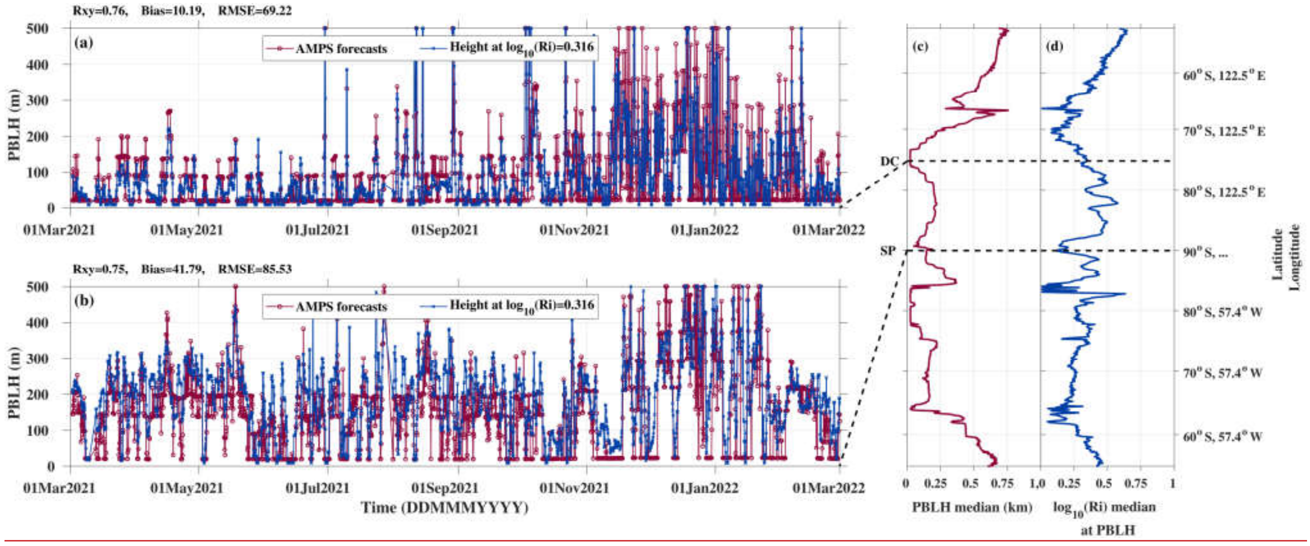


Figure 10. Temporal evolution of $PBLH$ directly forecasted by the AMPS (red circles) and estimated by the height corresponding to $\log_{10}(Ri)$ =0.316 (blue crosses) at DC (a) and SP (b). Median annual $PBLH$ (c) and $\log_{10}(Ri)$ at the $PBLH$ (d) along the red line through DC and SP shown in Fig. 7a.

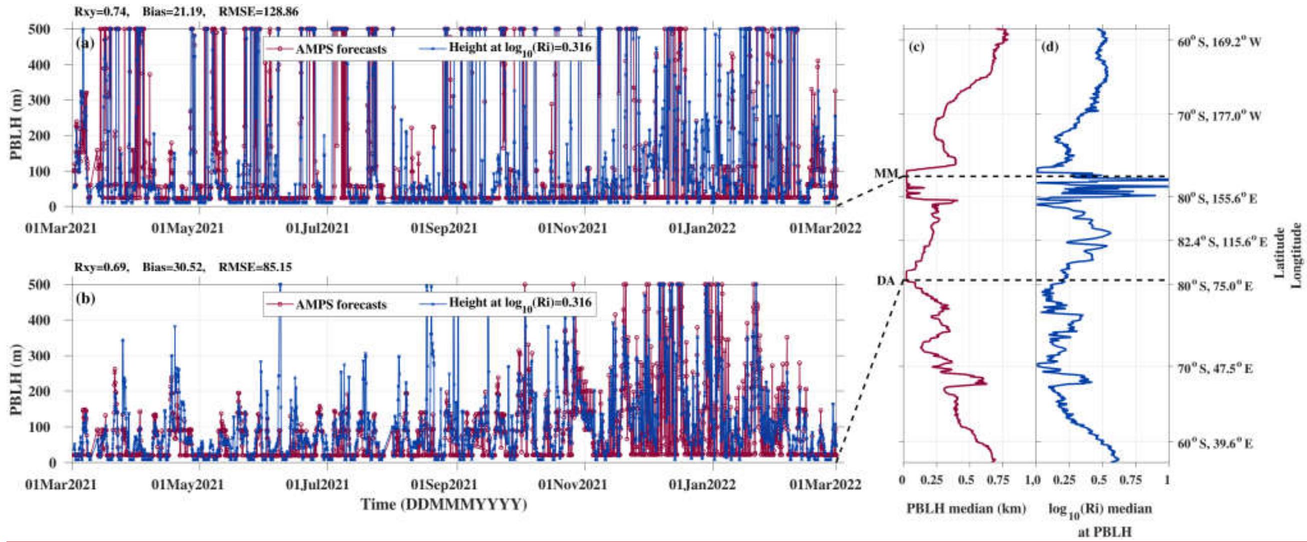


Figure 11. As in Fig. 10, but for data above MM and DA, plus the red line through MM and DA shown in Fig. 7b.

The ~~PBL~~planetary boundary layer scheme of Polar WRF in the AMPS ~~used~~was the Mellor-Yamada-Janjić (MYJ; Janjić, 1994) scheme, and the ability of the AMPS to model the Antarctic ~~PBL was~~ boundary layer has been examined by Wille et al. (2017). The MYJ scheme defines the $PBLH$ where turbulent kinetic energy decreases to a prescribed value of 0.1 $m^2\ s^{-2}$ ~~$m^2\ s^2$~~ (Xie et al., 2012)~~, and the~~. The AMPS forecasts include the values of $PBLH$. Figs. 10a ~~(DC)~~ and 11b ~~(DA)~~ show that the $PBLH$ directly forecasted by the AMPS ~~(red lines)~~ was mostly less than 100 m in the summit (DC and DA) during the polar winter, ~~which~~such variation range is consistent with the SODAR observations (DC: Petenko et al., 2014; DA: Bonner et al., 2010); Fig. 10b also displays a result being in accordance with the SODAR observations at the SP, as the most $PBLH$ was shown to be within 100-300 m (Travouillon et al., 2003). Thus, the AMPS-forecasted $PBLH$ is considered believable. to be realistic.

Figs. 10c and 11c show the median annual $PBLH$ forecasted by AMPS along the red lines in Figs. 7a and 7b, respectively. One can observe that the AMPS-forecasted is A thin $PBLH$ over the plateau can be observed, especially forat the summitsDomes (e.g., Dome ADA and Dome CDC), which agreesis consistent with previous studies (Swain and Gallée, 2006). WhileIn contrast, a thick $PBLH$ are is shown near the escarpment region, as seen by the dump in ~67 (e.g., ~68°S (up), 122.5°E in Fig. 10c and ~68°S (down) in Fig. 11c. This; this corresponds to the relatively low $Ri$ thick depth of near the large shown in enlarged drawings (Figs.ground in A11 area in Fig. 8 and 9).

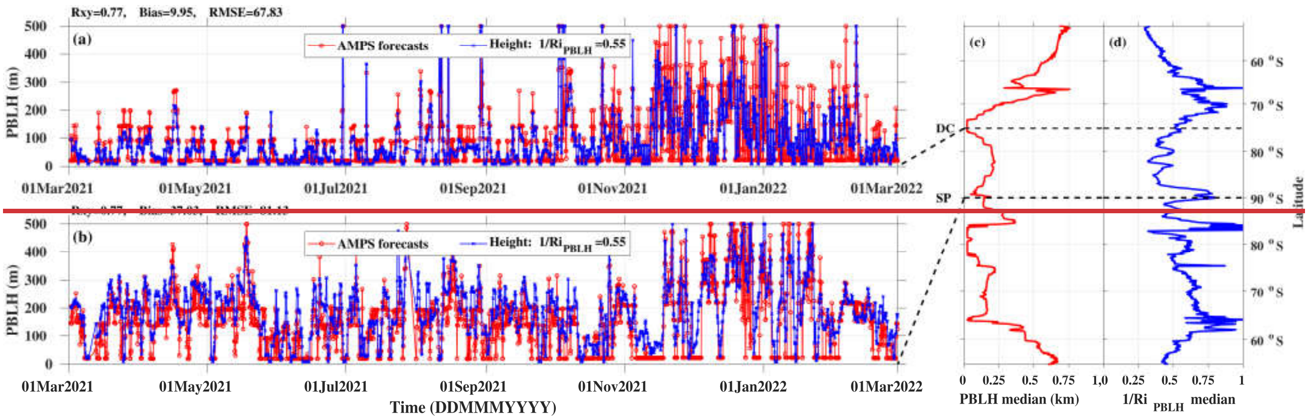


Figure 10. Temporal evolution of directly forecasted by the AMPS (red circles) and estimated by the height corresponding to ==0.55 (blue crosses) at DC (a) and SP (b). Median annual (c) and (d) along the red line through DC and SP shown in Fig. 7a.

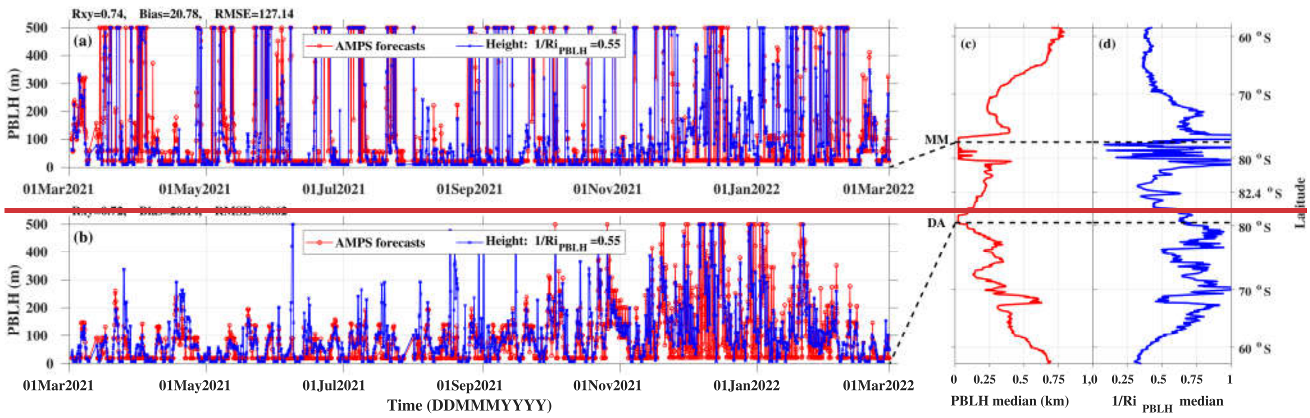


Figure 11. As in Fig. 10, but for data along the red line through MM and DA showed in Fig. 7b.

Then, The $\log_{10}\left(Ri_{PBLH}\right)$ was computed using linear interpolation between the AMPS grid with height equals to the AMPS-forecasted $PBLH$ .. The median value of $\log_{10}\left(Ri_{PBLH}\right)$ from the combined data of two vertical cross-sections (i.e. Figs. 10d and 11d) was calculated as 0.316, i.e., median $\log_{10}\left(Ri_{PBLH}\right)$ equals to 0.316 (or $Ri_{PBLH}$ 55 to give only one typical value.=2.07). However, some researchers have proposedemployed $Ri_{PBLH}$=0.25 () when radiosoundingsthe radiosonde measurements with the high vertical resolution arewas used (e.g. at Dome C; Pietroni et al., 2012). Here, the smaller critical valuelarger $Ri_{PBLH}$ for the

AMPS forecasts may be caused by the coarse vertical grid resolution (as implied from Troen and Mahrt, 1986)of the AMPS and its data smoothness (as mentioned in Sect. 4.2.1; the AMPS forecasts show smallerlarger $Ri$ than the radiosoundings thateven though they have already been interpolated to the same vertical resolution as the AMPS). grid).

To test the credibility of the critical value (i.e. $\log_{10}\left(Ri_{PBLH}\right)$=0.55316), $PBLH$ was also derived as the height where the AMPS-forecasted $\log_{10}\left(Ri\right)$ decreases to 0.316. The $R_{xy}$ , $Bias$ , and $RMSE$ 55 (blue lines in Figs. 10a-b and 11a-b). Even if larger critical values are used, no substantial variations would occur in the estimate because of the large gradient of near the ground (Fig. 4), also mentioned in . In the internal Antarctic Plateau (DC, SP, and DA), the shows a slight change in magnitude during the cold seasons (e.g. from March to October 2021). Such seasonal variation is not significant along the coast of Antarctica (MM), which fluctuates every season. During the polar summer (e.g. January 2022) at all four sites, estimated by =0.55 and read directly from the AMPS forecasts fluctuate considerably. The , , and of of $PBLH$ between the estimations using the critical value (=0.55) and AMPS forecasts,(blue lines in Figs. 10a-b and 11a-b) and the direct forecasts of AMPS (red lines in Figs. 10a-b and 11a-b) are depicted in the top left of the plot, where $Bias$ . indicates the former minus the latter. It appears that the values of $R_{xy}$ (> (all larger than 0.7269) are almost satisfactory, andthen we may conclude that $\log_{10}\left(Ri_{PBLH}\right)$ =0.55316 is a reliable critical value for judging the behaviourbehavior of atmospheric turbulence. The atmosphere layer could be considered turbulent whenfor $\log_{10}\left(Ri_{PBLH}\right)$ >≤0.55 (this 316 (when the turbulence intensity could be comparable to that within the boundary layer). However, this critical value may only be valid for using the AMPS forecasts). >9 indicates the results calculated by this critical value overestimate the . And >67 suggests that one should be careful when estimating a precise value for with this critical value (0.55)..

## 5 Discussion

The above results of the distribution provided us with valuable insights into the atmospheric turbulence in the Antarctic region. Here, we attempt to relate the features of atmospheric turbulence to some typical atmospheric conditions in Antarctica: temperature inversion, katabatic winds, and polar vortices.

The strength of the near-ground temperature inversion increases from the coast to the interior of Antarctica, and its strength weakens during summer (Fig. 2), such a phenomenon has also been observed in previous studies . Combined with the analysis of Figs. 11 and 12, the general increase in temperature-inversion strength was found to correspond to a less turbulent atmosphere with smaller (when the boundary layer is thinner), owing to large stability suppressing turbulence.

As a result of typical katabatic winds , the wind speeds increase from the interior plateau to the steep slope (Figs. 8 and 9). Strong winds can lead to increased levels of mechanical turbulence, as one can see a thick depth of large layer at the escarpment region.

A strong polar vortex means that zonal winds are strong, and atmospheric turbulence is more likely to be triggered. The Antarctic polar vortex reaches its peak intensity in the winter-spring and weakens during summer . One can also see that the free atmosphere in Antarctica becomes relatively calm during summer, as shown by the smaller in Figs. 8d and 9d. On the other hand, the strongest zonal winds exist over the ocean , which suggests that the atmosphere above the ocean can be an important source of turbulence (Figs. 8 and 9 show larger over the ocean).

## ~~6~~ Conclusion

We have examined the ability of AMPS to forecast the ~~inverse of the~~ Richardson number ~~(; the larger the , the higher the probability of triggering turbulence in the atmosphere)~~ in the Antarctic atmosphere. This includes ~~quantifying~~evaluating the accuracy of meteorological parameters ~~(Temperature~~( $\theta$ and $V$ ~~wind speed,~~, on which the $Ri$ depends), and comparing the $\log_{10}(Ri)$ ~~from the~~ estimations between radiosoundings and AMPS forecasts ~~and radiosoundings~~. In addition, the analysis of atmospheric $\log_{10}(Ri)$ over the entire Antarctic continent and the ocean surrounding it, was presented on an annual time scale. Finally, the $\log_{10}(Ri)$ at the Planetary Boundary Layer Height ( $PBLH$ ~~Further, the forecasted by the AMPS was employed to understand how to evaluate atmospheric stability or instability using the value of .~~) has been calculated.

From the analysis presented above, we deduce the following:

1. Comparisons of ~~the~~ AMPS forecasts with ~~the~~ radiosoundings from three representative sites (coast: McMurdo, flank: ~~the~~ South Pole, summit: Dome C) show that the forecasts can accurately describe the trend of atmospheric meteorological parameters above the Antarctic continent, as the $R_{xy}$ for $\theta$ reached as high as 0.99 and the $R_{xy}$ for $V$ ~~in almost the whole range from the ground to 25 km AGL. The monthly median difference in the air temperature is of the order of 1 K in a large part of the atmosphere, where the cold temperature bias occurs near the ground during winter. As for the wind speed, the median difference was ~ 1 m s$^{-1}$ and rarely exceeded 2 m s$^{-1}$.~~ are all larger than 0.85 (Table 2).

2. We proved that the AMPS forecasts can identify the main characteristics of atmospheric turbulence over the Antarctic continent in terms of both space and time. The $R_{xy}$ of $\log_{10}(Ri)$ at MM, SP, and DC are 0.71, 0.59, and 0.53, respectively. And the AMPS can reconstruct the near-ground "convex-concave–convex" shaped $\log_{10}(Ri)$ profiles indicated by the radiosonde measurements (Fig. 5). We also find that the $R_{xy}$ of $\log_{10}(Ri)$ would be higher when the $RMSE$ of $\theta$ and $V$ are smaller (Table 2). Besides, the AMPS can better capture the trend of $\log_{10}(Ri)$ ( $R_{xy}$ would be larger) at a relatively unstable atmosphere (weaker temperature inversion). Moreover, the values of $\log_{10}(Ri)$ ~~66, and 0.68, respectively, and larger was obtained during warm seasons. Moreover, the value of are all~~ were generally overestimated at the three sites; this is partly the result of the potential temperature gradients at the unstable atmosphere being overestimated by the AMPS, and the AMPS has generally underestimated ~~at these three sites. This may be because the model results are generally smoother than the measurements. Furthermore, a model depending on height to improve the AMPS-forecasted has been proposed~~the wind shear when it was strong.

3. The seasonal medians of the AMPS forecasts from two vertical cross-sections were presented~~,~~ (Figs. 8 and ~~the AMPS forecasts~~9). which provides us with a broader perspective on when and where atmospheric turbulence could be highly triggered in the Antarctic region. The AMPS-forecasted $\log_{10}(Ri)$ were qualitatively verified ~~again. it can be observed that~~ , as its statistical distribution behaved as the ~~AMPS can forecast the main~~expected atmospheric properties ~~as expected: strong temperature inversion near the ground,~~ attributed by some typical large-scale phenomena or local-scale dynamics (katabatic winds, polar vortices, convection, gravity wave, etc.) over the Antarctic plateau and the ocean surrounding it. For example, a very ~~calm~~laminar atmosphere ~~( is small) at high altitudes, and a thin boundary layer~~ above the Antarctic Plateau and a shallow boundary layer in the Domes area are illustrated by the AMPS forecasts.

4. The $\log_{10}(Ri)$ ~~, especially in the summit area. Moreover, we also obtained a new result, that strong wind shears near the escarpment regions have occurred from~~ at the $PBLH$ ~~ground to ~5 km AGL, causing a thick turbulent atmosphere with large~~

values of (or thick boundary layer), which is more evident during the polar winter. In addition, according to the temporal evolution of vertical cross-sections for a year from the video supplement, we find that unstable atmospheres are likely to be triggered over the ocean, move toward the Antarctic Plateau, and become stable.

4. The AMPS can forecast the boundary-layer height (). And the at the () was were calculated in this study, which could be a helpful reference standard for judging whether the atmospheric layer is stable (<) or unstable (>) when using AMPS-forecasted . The and their median value of from the combined data of two vertical cross-sections is 0.316, $\log_{10}(Ri)$=0.316 55, which has been in turn was used for estimating theto calculate $PBLH$ and agreesagree well with the AMPS-forecasted $PBLH$ ( $R_{xy} \geq$ 0.69). The atmosphere layer could be considered turbulent at $\log_{10}(Ri)$ (>0.72). <0.316 (when the turbulence intensity could be comparable to that within the boundary layer).

The overall results show that the AMPS can forecast thea realistic behaviour of $Ri$ and could be applied to, and the turbulence conditions in Antarctica are well revealed; furthermore, some practical operations that want to avoid a turbulent atmosphere — such as astronomical observations (Burton 2010), aviation safety (Gultepe and Feltz 2019) and free space optical communication (Jianjun Yin et al. 2017) — can apply the AMPS-forecasted $Ri$ astronomy in Antarctica, which is interested in the impacts of atmospheric turbulence ..

## Data availability

The meteorological parameters measured by radiosoundingsthe radiosondes at McMurdo, South Pole that support the findings of this study are available at the Antarctic Meteorological Research Center (ftp://amrc.ssec.wisc.edu/pub), while the meteorological parameters at Dome C are available at the Antarctic Meteo-Climatological Observatory (http://www.climantartide.it). The original WRF output files of AMPS used in this study can be found at https://www2.mmm.ucar.edu/rt/amps/information/amps_esg_data_info.html.

## Video supplement

The video supplement related to the vertical cross-section through the South Pole and Dome C in this article(Fig. 7a) is available online at https://doi.org/10.5446/60761. Another vertical cross-section through Dome A and McMurdo (Fig. 7b) is https://doi.org/10.5446/60760.

## Author contributions

QY and XW planned the investigation; QY, XH, XW, and ZW analyzed the data; QY and YG wrote the manuscript draft; QY finished the visualizition; QY, XW, XH, XQ, and ZW performed the valiation; XW, CQ, TL, XQ, and PW reviewed and edited the manuscript.

## Competing interests

The authors declare that they have no conflict of interest.

## Acknowledgments

This work was supported by the National Natural Science Foundation of China (grant ~~No. 91752103, 41576185~~Nos. 91752103, 41576185), Foundation of Key Laboratory of Science and Technology Innovation of Chinese Academy of Sciences (grant No. CXJJ-21S028) and the Foundation of Advanced Laser Technology Laboratory of Anhui Province (grant No. AHL2021QN02).

## References

Agabi, A., Aristidi, E., Azouit, M., Fossat, E., Martin, F., Sadibekova, T., Vernin, J., and Ziad, A.: First Whole Atmosphere Nighttime Seeing Measurements at Dome C, Antarctica, Publications of the Astronomical Society of the Pacific, 118, 344-348, 10.1086/498728, 2006.

Argentini, S., Pietroni, I., Mastrantonio, G., Viola, A. P., Dargaud, G., and Petenko, I.: Observations of near surface wind speed, temperature and radiative budget at Dome C, Antarctic Plateau during 2005, Antarctic Science, 26, 104-112, 10.1017/s0954102013000382, 2013.

Aristidi, E., Agabi, K., Azouit, M., Fossat, E., Vernin, J., Travouillon, T., Lawrence, J. S., Meyer, C., Storey, J. W. V., Halter, B., Roth, W. L., and Walden, V.: An analysis of temperatures and wind speeds above Dome C, Antarctica, Astronomy & Astrophysics, 430, 739-746, 10.1051/0004-6361:20041876, 2005.

Aristidi, E., Vernin, J., Fossat, E., Schmider, F. X., Travouillon, T., Pouzenc, C., Traullé, O., Genthon, C., Agabi, A., Bondoux, E., Challita, Z., Mékarnia, D., Jeanneaux, F., and Bouchez, G.: Monitoring the optical turbulence in the surface layer at Dome C, Antarctica, with sonic anemometers, Monthly Notices of the Royal Astronomical Society, 454, 4304-4315, 10.1093/mnras/stv2273, 2015.

Bonner, C. S., Ashley, M. C. B., Cui, X., Feng, L., Gong, X., Lawrence, J. S., Luong-Van, D. M., Shang, Z., Storey, J. W. V., Wang, L., Yang, H., Yang, J., Zhou, X., and Zhu, Z.: Thickness of the Atmospheric Boundary Layer Above Dome A, Antarctica, during 2009, Publications of the Astronomical Society of the Pacific, 122, 1122-1131, 10.1086/656250, 2010.

Boville, B. A., Kiehl, J. T., and Briegleb, B. P.: Evolution of the Antarctic polar vortex in spring: Response of a GCM to a prescribed Antarctic ozone hole, NASA, Goddard Space Flight Center, Polar Ozone Workshop., N89-14589, 224-227, https://ntrs.nasa.gov/citations/19890005218, 1988.

Bromwich, D. H., Otieno, F. O., Hines, K. M., Manning, K. W., and Shilo, E.: Comprehensive evaluation of polar weather research and forecasting model performance in the Antarctic, Journal of Geophysical Research: Atmospheres, 118, 274-292, 10.1029/2012jd018139, 2013.

Burton, M. G.: Astronomy in Antarctica, Astron. Astrophys. Rev., 18, 417-469, 10.1007/s00159-010-0032-2, 2010.

Chan, P. W.: Determination of Richardson number profile from remote sensing data and its aviation application, IOP Conference Series: Earth and Environmental Science 1, 012043, 10.1088/1755-1307/1/1/012043, 2008.

Deardorff, J. W.: On the entrainment rate of a stratocumulus-topped mixed layer, Quarterly Journal of the Royal Meteorological Society, 102, 563-582, 10.1002/qj.49710243306, 1976.

Gallée, H., Preunkert, S., Argentini, S., Frey, M. M., Genthon, C., Jourdain, B., Pietroni, I., Casasanta, G., Barral, H., Vignon, E., Amory, C., and Legrand, M.: Characterization of the boundary layer at Dome C (East Antarctica) during the OPALE summer campaign, Atmos. Chem. Phys., 15, 6225-6236, 10.5194/acp-15-6225-2015, 2015.

Geissler, K. and Masciadri, E.: Meteorological Parameter Analysis above Dome C Using Data from the European Centre for Medium-Range Weather Forecasts, Publications of the Astronomical Society of the Pacific, 118, 1048-1065, 10.1086/505891, 2006.

Gultepe, I. and Feltz, W. F.: Aviation Meteorology: Observations and Models. Introduction, Pure and Applied Geophysics, 176, 1863-1867, 10.1007/s00024-019-02188-2, 2019.

Guo, J., Zhang, J., Yang, K., Liao, H., Zhang, S., Huang, K., Lv, Y., Shao, J., Yu, T., Tong, B., Li, J., Su, T., Yim, S. H. L., Stoffelen, A., Zhai, P., and Xu, X.: Investigation of near-global daytime boundary layer height using high-resolution radiosondes: first results and comparison with ERA5, MERRA-2, JRA-55, and NCEP-2 reanalyses, Atmos. Chem. Phys., 21, 17079-17097, 10.5194/acp-21-17079-2021, 2021.

Hagelin, S., Masciadri, E., Lascaux, F., and Stoesz, J.: Comparison of the atmosphere above the South Pole, Dome C and Dome A: first attempt, Monthly Notices of the Royal Astronomical Society, 387, 1499-1510, 10.1111/j.1365-2966.2008.13361.x, 2008.

Han, Y., Yang, Q., Liu, N., Zhang, K., Qing, C., Li, X., Wu, X., and Luo, T.: Analysis of wind-speed profiles and optical turbulence above Gaomeigu and the Tibetan Plateau using ERA5 data, Monthly Notices of the Royal Astronomical Society, 501, 4692-4702, 10.1093/mnras/staa2960, 2021.

He, Y., Sheng, Z., and He, M.: The First Observation of Turbulence in Northwestern China by a Near-Space High-Resolution Balloon Sensor, Sensors, 20, 677, 10.3390/s20030677, 2020.

Hines, K. M. and Bromwich, D. H.: Development and Testing of Polar Weather Research and Forecasting (WRF) Model. Part I: Greenland Ice Sheet Meteorology*, Monthly Weather Review, 136, 1971-1989, 10.1175/2007mwr2112.1, 2008.

Hines, K. M., Bromwich, D. H., Bai, L., Bitz, C. M., Powers, J. G., and Manning, K. W.: Sea Ice Enhancements to Polar WRF*, Monthly Weather Review, 143, 2363-2385, 10.1175/mwr-d-14-00344.1, 2015.

Hines, K. M., Bromwich, D. H., Wang, S.-H., Silber, I., Verlinde, J., and Lubin, D.: Microphysics of summer clouds in central West Antarctica simulated by the Polar Weather Research and Forecasting Model (WRF) and the Antarctic Mesoscale Prediction System (AMPS), Atmospheric Chemistry and Physics, 19, 12431-12454, 10.5194/acp-19-12431-2019, 2019.

Holtslag, A. A. M., de Bruijn, E. I. F., and Pan, H.-L.: A High Resolution Air Mass Transformation Model for Short-Range Weather Forecasting, Monthly Weather Review, 118, 1561, 10.1175/1520-0493(1990)118<1561:Ahramt>2.0.Co;2, 1990.

Hu, Y., Hu, K., Shang, Z., Ashley, M. C. B., Ma, B., Du, F., Li, Z., Liu, Q., Wang, W., Yang, S., Yu, C., and Zeng, Z.: Meteorological Data from KLAWS-2G for an Astronomical Site Survey of Dome A, Antarctica, Publications of the Astronomical Society of the Pacific, 131, 015001, 10.1088/1538-3873/aae916, 2019.

Huang, T., Yang, Y., O'Connor, E. J., Lolli, S., Haywood, J., Osborne, M., Cheng, J. C.-H., Guo, J., and Yim, S. H.-L.: Influence of a weak typhoon on the vertical distribution of air pollution in Hong Kong: A perspective from a Doppler LiDAR network, Environmental Pollution, 276, 116534, 10.1016/j.envpol.2021.116534, 2021.

Hudson, S. R. and Brandt, R. E.: A Look at the Surface-Based Temperature Inversion on the Antarctic Plateau, Journal of Climate, 18, 1673-1696, 10.1175/jcli3360.1, 2005.

Janjić, Z. I.: The Step-Mountain Eta Coordinate Model: Further Developments of the Convection, Viscous Sublayer, and Turbulence Closure Schemes, Monthly Weather Review, 122, 927-945, 10.1175/1520-0493(1994)122<0927:Tsmecm>2.0.Co;2, 1994.

Kantha, L., Luce, H., and Hashiguchi, H.: Midlevel Cloud-Base Turbulence: Radar Observations and Models, Journal of Geophysical Research: Atmospheres, 124, 3223-3245, 10.1029/2018JD029479, 2019.

Karpetchko, A., Kyrö, E., and Knudsen, B. M.: Arctic and Antarctic polar vortices 1957–2002 as seen from the ERA-40 reanalyses, Journal of Geophysical Research, 110, 10.1029/2005jd006113, 2005.

Kudo, A.: The Generation of Turbulence below Midlevel Cloud Bases: The Effect of Cooling due to Sublimation of Snow, Journal of Applied Meteorology and Climatology, 52, 819-833, 10.1175/jamc-d-12-0232.1, 2013.

Lascaux, F., Masciadri, E., Hagelin, S., and Stoesz, J.: Mesoscale optical turbulence simulations at Dome C, Monthly Notices of the Royal Astronomical Society, 398, 1093-1104, 10.1111/j.1365-2966.2009.15151.x, 2009.

Listowski, C. and Lachlan-Cope, T.: The microphysics of clouds over the Antarctic Peninsula – Part 2: modelling aspects within Polar WRF, Atmospheric Chemistry and Physics, 17, 10195-10221, 10.5194/acp-17-10195-2017, 2017.

Lv, Y., Guo, J., Li, J., Cao, L., Chen, T., Wang, D., Chen, D., Han, Y., Guo, X., Xu, H., Liu, L., Solanki, R., and Huang, G.: Spatiotemporal characteristics of atmospheric turbulence over China estimated using operational high-resolution soundings, Environmental Research Letters, 16, 054050, 10.1088/1748-9326/abf461, 2021.

Ma, B., Shang, Z., Hu, Y., Hu, K., Wang, Y., Yang, X., Ashley, M. C. B., Hickson, P., and Jiang, P.: Night-time measurements of astronomical seeing at Dome A in Antarctica, Nature, 583, 771-774, 10.1038/s41586-020-2489-0, 2020.

Ma, Y., Bian, L., Xiao, C., Allison, I., and Zhou, X.: Near surface climate of the traverse route from Zhongshan Station to Dome A, East Antarctica, Antarctic Science, 22, 443-459, 10.1017/s0954102010000209, 2010.

Marks, R. D., Vernin, J., Azouit, M., Manigault, J. F., and Clevelin, C.: Measurement of optical seeing on the high antarctic plateau, Astronomy and Astrophysics Supplement Series, 134, 161-172, 10.1051/aas:1999100, 1999.

Mihalikova, M., Kirkwood, S., Arnault, J., and Mikhaylova, D.: Observation of a tropopause fold by MARA VHF wind-profiler radar and ozonesonde at Wasa, Antarctica: comparison with ECMWF analysis and a WRF model simulation, Ann. Geophys., 30, 1411-1421, 10.5194/angeo-30-1411-2012, 2012.

Monaghan, A. J., Bromwich, D. H., Powers, J. G., and Manning, K. W.: The Climate of the McMurdo, Antarctica, Region as Represented by One Year of Forecasts from the Antarctic Mesoscale Prediction System, Journal of Climate, 18, 1174-1189, 10.1175/JCLI3336.1, 2005.

Nigro, M. A., Cassano, J. J., Wille, J., Bromwich, D. H., and Lazzara, M. A.: A Self-Organizing-Map-Based Evaluation of the Antarctic Mesoscale Prediction System Using Observations from a 30-m Instrumented Tower on the Ross Ice Shelf, Antarctica, Weather and Forecasting, 32, 223-242, 10.1175/waf-d-16-0084.1, 2017.

P. Lönnberg, D. B. S.: ECMWF Data Assimilation - scientific documentation, 3rd ed., Shinfield Park, Reading, 1992.

Parish, T. R. and Waight, K. T.: The Forcing of Antarctic Katabatic Winds, Monthly Weather Review, 115, 2214-2226, 10.1175/1520-0493(1987)115<2214:TFOAKW>2.0.CO;2, 1987.

Petenko, I., Argentini, S., Casasanta, G., Genthon, C., and Kallistratova, M.: Stable Surface-Based Turbulent Layer During the Polar Winter at Dome C, Antarctica: Sodar and In Situ Observations, Boundary-Layer Meteorology, 171, 101-128, 10.1007/s10546-018-0419-6, 2019.

Petenko, I., Argentini, S., Pietroni, I., Viola, A., Mastrantonio, G., Casasanta, G., Aristidi, E., Bouchez, G., Agabi, A., and Bondoux, E.: Observations of optically active turbulence in the planetary boundary layer by sodar at the Concordia astronomical observatory, Dome C, Antarctica, Astronomy & Astrophysics, 568, 10.1051/0004-6361/201323299, 2014.

Pietroni, I., Argentini, S., Petenko, I., and Sozzi, R.: Measurements and Parametrizations of the Atmospheric Boundary-Layer Height at Dome C, Antarctica, Boundary-Layer Meteorology, 143, 189-206, 10.1007/s10546-011-9675-4, 2012.

Powers, J. G., Manning, K. W., Bromwich, D. H., Cassano, J. J., and Cayette, A. M.: A Decade of Antarctic Science Support Through Amps, Bulletin of the American Meteorological Society, 93, 1699-1712, 10.1175/bams-d-11-00186.1, 2012.

Richardson, L. F. and Shaw, W. N.: The supply of energy from and to atmospheric eddies, Proceedings of the Royal Society of London. Series A, Containing Papers of a Mathematical and Physical Character, 97, 354-373, doi:10.1098/rspa.1920.0039, 1920.

Rinke, A., Ma, Y., Bian, L., Xin, Y., Dethloff, K., Persson, P. O. G., Lüpkes, C., and Xiao, C.: Evaluation of atmospheric boundary layer-surface process relationships in a regional climate model along an East Antarctic traverse, Journal of Geophysical Research: Atmospheres, 117, n/a-n/a, 10.1029/2011jd016441, 2012.

Saunders, W., Lawrence, J. S., Storey, J. W. V., Ashley, M. C. B., Kato, S., Minnis, P., Winker, D. M., Liu, G., and Kulesa, C.: Where Is the Best Site on Earth? Domes A, B, C, and F, and Ridges A and B, Publications of the Astronomical Society of the Pacific, 121, 976-992, 10.1086/605780, 2009.

Seefeldt, M. W., Cassano, J. J., and Nigro, M. A.: A Weather-Pattern-Based Approach to Evaluate the Antarctic Mesoscale Prediction System (AMPS) Forecasts: Comparison to Automatic Weather Station Observations, Weather and Forecasting, 26, 184-198, 10.1175/2010waf2222444.1, 2011.

Solanki, R., Guo, J., Lv, Y., Zhang, J., Wu, J., Tong, B., and Li, J.: Elucidating the atmospheric boundary layer turbulence by combining UHF radar wind profiler and radiosonde measurements over urban area of Beijing, Urban Climate, 43, 101151, 10.1016/j.uclim.2022.101151, 2022.

Spinhirne, J. D., Palm, S. P., and Hart, W. D.: Antarctica cloud cover for October 2003 from GLAS satellite lidar profiling, Geophysical Research Letters, 32, 10.1029/2005GL023782, 2005.

Sun, B., Reale, T., Schroeder, S., Pettey, M., and Smith, R.: On the Accuracy of Vaisala RS41 versus RS92 Upper-Air Temperature Observations, Journal of Atmospheric and Oceanic Technology, 36, 635-653, 10.1175/jtech-d-18-0081.1, 2019.

Sun, B., Calbet, X., Reale, A., Schroeder, S., Bali, M., Smith, R., and Pettey, M.: Accuracy of Vaisala RS41 and RS92 Upper Tropospheric Humidity Compared to Satellite Hyperspectral Infrared Measurements, Remote Sensing, 13, 173, 10.3390/rs13020173, 2021.

Swain, Mark R. and Gallée, H.: Antarctic Boundary Layer Seeing, Publications of the Astronomical Society of the Pacific, 118, 1190-1197, 10.1086/507153, 2006.

Town, M. S. and Walden, V. P.: Surface energy budget over the South Pole and turbulent heat fluxes as a function of an empirical bulk Richardson number, Journal of Geophysical Research, 114, 10.1029/2009jd011888, 2009.

Travouillon, T., Ashley, M. C. B., Burton, M. G., Storey, J. W. V., and Loewenstein, R. F.: Atmospheric turbulence at the South Pole and its implications for astronomy, Astronomy & Astrophysics, 400, 1163-1172, 10.1051/0004-6361:20021814, 2003.

Trinquet, H., Agabi, A., Vernin, J., Azouit, M., Aristidi, E., and Fossat, E.: Nighttime Optical Turbulence Vertical Structure above Dome C in Antarctica, Publications of the Astronomical Society of the Pacific, 120, 203-211, 10.1086/528808, 2008.

Troen, I. B. and Mahrt, L.: A simple model of the atmospheric boundary layer; sensitivity to surface evaporation, Boundary-Layer Meteorology, 37, 129-148, 10.1007/BF00122760, 1986.

Vázquez B, G. E. and Grejner-Brzezinska, D. A.: GPS-PWV estimation and validation with radiosonde data and numerical weather prediction model in Antarctica, GPS Solutions, 17, 29-39, 10.1007/s10291-012-0258-8, 2012.

Verma, M. K., Kumar, A., and Pandey, A.: Phenomenology of buoyancy-driven turbulence: recent results, New Journal of Physics, 19, 025012, 10.1088/1367-2630/aa5d63, 2017.

Vernin, J., Chadid, M., Aristidi, E., Agabi, A., Trinquet, H., and Van der Swaelmen, M.: First single star scidar measurements at Dome C, Antarctica, Astronomy & Astrophysics, 500, 1271-1276, 10.1051/0004-6361/200811119, 2009.

Wille, J. D., Bromwich, D. H., Cassano, J. J., Nigro, M. A., Mateling, M. E., and Lazzara, M. A.: Evaluation of the AMPS Boundary Layer Simulations on the Ross Ice Shelf, Antarctica, with Unmanned Aircraft Observations, Journal of Applied Meteorology and Climatology, 56, 2239-2258, 10.1175/jamc-d-16-0339.1, 2017.

Wille, J. D., Bromwich, D. H., Nigro, M. A., Cassano, J. J., Mateling, M., Lazzara, M. A., and Wang, S.-H.: Evaluation of the AMPS Boundary Layer Simulations on the Ross Ice Shelf with Tower Observations, Journal of Applied Meteorology and Climatology, 55, 2349-2367, 10.1175/jamc-d-16-0032.1, 2016.

Xie, B., Fung, J. C. H., Chan, A., and Lau, A.: Evaluation of nonlocal and local planetary boundary layer schemes in the WRF model, Journal of Geophysical Research: Atmospheres, 117, n/a-n/a, 10.1029/2011jd017080, 2012.

Xue, H., Giorgetta, M. A., and Guo, J.: The daytime trapped lee wave pattern and evolution induced by two small-scale mountains of different heights, Quarterly Journal of the Royal Meteorological Society, 148, 1300-1318, 10.1002/qj.4262, 2022.

Yagüe, C., Maqueda, G., and Rees, J. M.: Characteristics of turbulence in the lower atmosphere at Halley IV station, Antarctica, Dynamics of Atmospheres & Oceans, 34, 205-223, 10.1016/S0377-0265(01)00068-9, 2001.

Yang, Q., Wu, X., Wang, Z., Hu, X., Guo, Y., and Qing, C.: Simulating the night-time astronomical seeing at Dome A using Polar WRF, Monthly Notices of the Royal Astronomical Society, 515, 1788-1794, 10.1093/mnras/stac1930, 2022.

Yang, Q., Wu, X., Han, Y., Qing, C., Wu, S., Su, C., Wu, P., Luo, T., and Zhang, S.: Estimating the astronomical seeing above Dome A using Polar WRF based on the Tatarskii equation, Optics Express, 29, 44000-44011, 10.1364/oe.439819, 2021.

Zhang, J., Guo, J., Zhang, S., and Shao, J.: Inertia-gravity wave energy and instability drive turbulence: evidence from a near-global high-resolution radiosonde dataset, Climate Dynamics, 58, 2927-2939, 10.1007/s00382-021-06075-2, 2022a.

Zhang, J., Guo, J., Xue, H., Zhang, S., Huang, K., Dong, W., Shao, J., Yi, M., and Zhang, Y.: Tropospheric Gravity Waves as Observed by the High-Resolution China Radiosonde Network and Their Potential Sources, Journal of Geophysical Research: Atmospheres, 127, e2022JD037174, 10.1029/2022JD037174, 2022b.

Zuev, V. V. and Savelieva, E.: The cause of the strengthening of the Antarctic polar vortex during October–November periods, Journal of Atmospheric and Solar-Terrestrial Physics, 190, 1-5, 10.1016/j.jastp.2019.04.016, 2019a.

Zuev, V. V. and Savelieva, E.: The cause of the spring strengthening of the Antarctic polar vortex, Dynamics of Atmospheres and Oceans, 87, 10.1016/j.dynatmoce.2019.101097, 2019b.